

Increased acceptance bandwidths in optical frequency conversion by use of multiple walk-off-compensating nonlinear crystals

A. V. Smith, D. J. Armstrong,* and W. J. Alford

Department of Lasers, Optics, and Remote Sensing, Sandia National Laboratories, Albuquerque, New Mexico 87185-1423

Received April 29, 1997; revised manuscript received August 13, 1997

We show by experiment and mathematical model that angular and frequency acceptance bandwidths for frequency mixing in a nonlinear crystal can often be improved by segmenting the crystal and reversing the spatial or temporal walk-off in alternating segments. We analyze nonlinear mixing primarily in real space, (x, t) , rather than Fourier space, (k, ω) , and show that acceptance bands for sum- and difference-frequency mixing can be increased by up to a factor equal to the number of crystal segments. We consider both high- and low-efficiency mixing as well as parametric gain, and show that in many cases of practical interest the increased bandwidth substantially improves conversion efficiency. We also attempt to clarify the role of acceptance bandwidths in frequency mixing. © 1998 Optical Society of America [S0740-3224(98)02301-7]

OCIS codes: 190.0190, 190.2620, 190.4410, 190.7110, 190.4420, 320.7110.

1. INTRODUCTION

The efficiency of frequency conversion by parametric mixing in a nonlinear crystal is often limited by the crystal's angular or frequency acceptance band, or equivalently, by its birefringent or group-velocity walk-off. In certain cases, the acceptance bands can be increased and the walk-offs lessened by use of multiple walk-off-compensating crystals. For example, angle-critical phase matching can be made to approximate noncritical phase matching by dividing the crystal into a number of short segments arranged so that alternate segments have opposite birefringence-induced walk-off directions. The segments are individually critically phase matched, in contrast to the very short non-phase-matched segments typical of quasi-phase matching, which also has the large acceptance angles characteristic of noncritical phase matching. Similarly, frequency bandwidth limitations are relaxed if alternate segments have opposite temporal, or group-velocity, walk-off. Besides improving mixing efficiency, temporal walk-off compensation alleviates the problem of pulse stretching for very short pulses. Achieving temporal compensation is not as straightforward as spatial compensation because one cannot simply reverse the orientation of alternating crystal segments. However, the compensating segments need not contribute directly to mixing. For example, in frequency doubling with a negative uniaxial crystal such as β -barium borate (BBO), alternate crystal segments could be tuned away from the phase-matching angle to the point where the group-velocity mismatch is reversed. These passive segments might also provide spatial walk-off compensation. We note for completeness that there are other ways of matching group velocities such as quasi-phase matching¹ or noncollinear phase matching.² Finally, the tempera-

ture bandwidth of a crystal could be increased by reversing the temperature coefficient of phase mismatch in alternate segments.

Considerable prior work has focused on the use of two crystals oriented to compensate spatial walk-off to improve frequency-doubling efficiency³⁻⁹ and parametric-oscillator performance.^{10,11} Some of this work has also addressed the key issue of the signs of the effective nonlinear coefficients in the two segments.^{3,4,11,12} Additionally, Xijie *et al.*¹³ showed that the acceptance angle is doubled for two walk-off-compensated crystals. Walk-off compensation in more than two crystals has been demonstrated in experiments by Andreev *et al.*, who present measurements of second-harmonic generation by means of a beam with a spherical phase front passing through one to five crystals to demonstrate improved mixing efficiency, and by Zondy *et al.*,¹⁴ who used four optically contacted potassium titanyl phosphate (KTP) crystals to frequency double 2529-nm light. We extend these works by presenting calculations that quantify the benefits of walk-off compensation, including the case of high-conversion limit, for which the benefits can be especially significant. These are supplemented with laboratory demonstrations of enhanced mixing efficiency and increased acceptance angle for beams with various mode profiles, obtained by two to four walk-off-compensating crystals. We also extend the idea of compensation to temporal walk-off and show how it broadens the frequency bandwidth.

To provide a foundation for our discussions, we briefly review some standard methods of analysis for parametric mixing in critically phase-matched and dispersive crystals. We then apply these methods to several illustrative cases that demonstrate the benefits of walk-off compensation, and we support our analyses with laboratory results.

2. REVIEW OF ANALYSIS METHODS

Parametric mixing can be analyzed either in terms of the monochromatic plane waves that are the Fourier components of light beams, or more directly in terms of the spatial and temporal profiles of the beams. The former description, in terms of $E(k_x, k_y, z, \omega)$, we refer to as the Fourier picture, while the latter description, in terms of $E(x, y, z, t)$, we term the local picture. In a uniaxial crystal or for propagation in one of the principal planes of a biaxial crystal, birefringence is manifest in the Fourier picture as an angular dependence of the refractive index for extraordinary or *e*-polarized plane waves. Similarly, group velocity in the Fourier picture is associated with a frequency dependence of the refractive index. The refractive index for ordinary or *o*-polarized plane waves also depends on frequency but is independent of propagation direction. The equations describing parametric mixing in terms of monochromatic plane waves with wave vector $\mathbf{k} = k_x \hat{\mathbf{x}} + k_y \hat{\mathbf{y}} + k_z \hat{\mathbf{z}}$ and frequency $\omega = \omega_0 + \Delta\omega$ can be written in the slowly varying amplitude and quasi-monochromatic approximations as¹⁵⁻¹⁸

$$\left[\frac{\partial}{\partial z} + \frac{i}{2k_1} (k_x^2 + k_y^2) + i\alpha_1 (\Delta\omega)^2 + \frac{i\Delta\omega}{v_1} + ik_x \rho_1 \right] \epsilon_1(k_x, k_y, z, \Delta\omega) = P_1(k_x, k_y, z, \Delta\omega), \quad (1)$$

$$\left[\frac{\partial}{\partial z} + \frac{i}{2k_2} (k_x^2 + k_y^2) + i\alpha_2 (\Delta\omega)^2 + \frac{i\Delta\omega}{v_2} + ik_x \rho_2 \right] \epsilon_2(k_x, k_y, z, \Delta\omega) = P_2(k_x, k_y, z, \Delta\omega), \quad (2)$$

$$\left[\frac{\partial}{\partial z} + \frac{i}{2k_3} (k_x^2 + k_y^2) + i\alpha_3 (\Delta\omega)^2 + \frac{i\Delta\omega}{v_3} + ik_x \rho_3 \right] \epsilon_3(k_x, k_y, z, \Delta\omega) = P_3(k_x, k_y, z, \Delta\omega), \quad (3)$$

where the nonlinear polarization terms P_n are the convolution integrals

$$P_1(k_x, k_y, z, \Delta\omega) = i \frac{d_{\text{eff}} \omega_1}{c n_1} \iiint \exp(i\Delta k z) \epsilon_2^*(k'_x, k'_y, z, \delta) \times \epsilon_3(k_x + k'_x, k_y + k'_y, z, \Delta\omega + \delta) dk'_x dk'_y d\delta, \quad (4)$$

$$P_2(k_x, k_y, z, \Delta\omega) = i \frac{d_{\text{eff}} \omega_2}{c n_2} \iiint \exp(i\Delta k z) \epsilon_1^*(k'_x, k'_y, z, \delta) \times \epsilon_3(k_x + k'_x, k_y + k'_y, z, \Delta\omega + \delta) dk'_x dk'_y d\delta, \quad (5)$$

$$P_3(k_x, k_y, z, \Delta\omega) = i \frac{d_{\text{eff}} \omega_3}{c n_3} \iiint \exp(-i\Delta k z) \epsilon_2(k_x - k'_x, k_y - k'_y, z, \Delta\omega - \delta) \epsilon_1(k'_x, k'_y, z, \delta) dk'_x dk'_y d\delta, \quad (6)$$

The ϵ 's are Fourier-field amplitudes of the monochromatic plane waves, the subscripts 1, 2, and 3 refer to three waves satisfying $\omega_1 + \omega_2 = \omega_3$, and $\Delta k = k_{3z} - k_{1z} - k_{2z}$ is the phase-velocity mismatch, where $k_i = n_i \omega_i / c$. The n 's are refractive indexes, d_{eff} is the effective nonlinear coefficient, the ρ 's are birefringent walk-off angles, the v 's are group velocities, and the α 's are intrapulse group-velocity-dispersion coefficients. In this paper we will assume negligible group-velocity dispersion and set the α 's equal to zero. The convolution integrals express the reasonable notion that each polarization wave has contributions from all pairs of radiation waves whose transverse k vectors and frequency shifts add to produce those of the polarization wave.

Fourier transforming these equations gives the corresponding parametric mixing equations in the local picture, that is, in terms of $\epsilon(x, y, z, t)$ rather than $\epsilon(k_x, k_y, z, \Delta\omega)$:

$$\left[\frac{\partial}{\partial z} - \frac{i}{2k_1} \left(\frac{\partial^2}{\partial x^2} + \frac{\partial^2}{\partial y^2} \right) + i\alpha_1 \frac{\partial^2}{\partial t^2} + \frac{1}{v_1} \frac{\partial}{\partial t} + \rho_1 \frac{\partial}{\partial x} \right] \times \epsilon_1(x, y, z, t) = \frac{i\omega_1 d_{\text{eff}}}{n_1 c} \epsilon_3(x, y, z, t) \epsilon_2^*(x, y, z, t) \exp(i\Delta k_0 z), \quad (7)$$

$$\left[\frac{\partial}{\partial z} - \frac{i}{2k_2} \left(\frac{\partial^2}{\partial x^2} + \frac{\partial^2}{\partial y^2} \right) + i\alpha_2 \frac{\partial^2}{\partial t^2} + \frac{1}{v_2} \frac{\partial}{\partial t} + \rho_2 \frac{\partial}{\partial x} \right] \times \epsilon_2(x, y, z, t) = \frac{i\omega_2 d_{\text{eff}}}{n_2 c} \epsilon_3(x, y, z, t) \epsilon_1^*(x, y, z, t) \exp(i\Delta k_0 z), \quad (8)$$

$$\left[\frac{\partial}{\partial z} - \frac{i}{2k_3} \left(\frac{\partial^2}{\partial x^2} + \frac{\partial^2}{\partial y^2} \right) + i\alpha_3 \frac{\partial^2}{\partial t^2} + \frac{1}{v_3} \frac{\partial}{\partial t} + \rho_3 \frac{\partial}{\partial x} \right] \times \epsilon_3(x, y, z, t) = \frac{i\omega_3 d_{\text{eff}}}{n_3 c} \epsilon_2(x, y, z, t) \epsilon_1(x, y, z, t) \exp(-i\Delta k_0 z). \quad (9)$$

In both sets of mixing equations, the second term on the left side accounts for diffraction. The effect of birefringence is to tilt the Poynting vector of *e*-polarized beams by ρ relative to \mathbf{k} , where

$$\rho = -\frac{1}{n_e} \frac{dn_e}{d\theta}. \quad (10)$$

This angle between the wave vector and the Poynting vector leads to a spatial walk-off of ρz for beams with extraordinary polarization. The form of Eq. (10) makes evi-

dent the general inverse relationship between the plane-wave acceptance angle, proportional to $(dn_e/d\theta)^{-1}$, and the walk-off angle ρ .

Group velocity refers to the propagation speed of light pulses and is defined by

$$\frac{1}{v} = \frac{n}{c} + \frac{\omega}{c} \frac{dn}{d\omega} = \frac{dk}{d\omega}. \quad (11)$$

The propagation time over a length L is L/v , so a variation in group velocities leads to a temporal separation of pulses of different polarization or wavelength. The form of Eq. (11) makes apparent the inverse relationship between acceptance bandwidth, proportional to $(dk/d\omega)^{-1}$, and the temporal walk-off between pulses.

We want to stress two points regarding the application of the parametric-mixing equations. First, although mixing can be analyzed with equal validity in the Fourier (k, ω) or the local (x, t) description, the latter is more intuitive and less prone to misinterpretation. In applying the Fourier description, it is essential to correctly assign the phase as well as the amplitude of each component plane wave. Furthermore, to account for nonlinear coupling these component plane waves must be combined in the convolution integrals, and Δk must be evaluated. These steps are not easily visualized except in very simple cases such as monochromatic plane waves. In contrast, all effects of acceptance angle and acceptance bandwidth are accounted for in the local description in terms of local amplitudes and phases, combined with spatial or temporal walk-off. The spatial walk-off term in Eqs. (7)–(9) causes a lateral translation of an e -polarized beam in the direction of walk-off as it propagates through the crystal. Similarly, the group-velocity term causes a temporal translation. Note that no explicit angular or frequency dependence of n appears in the local equations and that both ρ and Δk_0 are those of a carrier plane wave of frequency ω_0 propagating in the \hat{z} direction. Phase shifts caused by the combination of local wave-front tilt and spatial walk-off completely account for the angular dependence of n , while those that are due to the combination of temporal phase structure and temporal walk-off account for the frequency dependence of n . Because it is less prone to misinterpretation, we prefer the local description in this paper, but we will show how the description in terms of Fourier components derives from it.

The second point of emphasis involves the mathematical similarities between temporal and spatial walk-off and between diffraction and group-velocity dispersion. For example, in frequency doubling a beam with Gaussian spatial and temporal profiles, spatial walk-off affects the spatial profile and its Fourier transform, the angular spectrum, in the same way temporal walk-off affects the temporal profile and its transform, the frequency spectrum, assuming negligible diffraction and group-velocity dispersion. We will use this equivalence throughout this paper, giving examples of each and pointing out the analogies of each with the other.

3. LOW-CONVERSION LIMIT

In this section we apply the methods above to several illustrative examples in four categories. The first category

is plane waves, an appropriate approximation for beams with confocal lengths much greater than the crystal length, diameters large compared with the spatial walk-off, and pulse durations long compared with temporal walk-off. The second is collimated Gaussian beams, again with confocal lengths much greater than the crystal length, but with beam diameters comparable to the spatial walk-off. The same analysis also applies to pulses with durations comparable to the temporal walk-off. The third is focused Gaussian beams, where the confocal parameter is comparable to the crystal length, and the fourth is beams spatially structured on a scale comparable with that of the spatial walk-off, or temporally structured on a scale comparable with that of the temporal walk-off. To treat these cases, we developed several tools for analysis. One is a computational model based on numeric integration of the mixing equations, including diffraction and spatial walk-off but not temporal walk-off. This is described more completely in a previous paper.¹⁹ A second is a similar model including temporal walk-off but not diffraction or spatial walk-off. Both models are applicable at high-conversion efficiency as well as at low. The single-crystal version of these models are included in the software package SNLO.²⁰ Finally, we extended the analytic results of Boyd and Kleinman²¹ for low-conversion second-harmonic generation with focused Gaussian beams to include walk-off compensation in two crystal segments.

A. Plane Waves

We use the well-known monochromatic plane-wave solutions for frequency doubling in critically phase-matched crystals to show that the acceptance angle for N walk-off-compensating crystal segments, each of length L/N , is N times that of a single crystal of length L . For a single crystal of length L , the harmonic field is given by²²

$$\epsilon_{2\omega} = i \frac{\omega d_{\text{eff}}}{nc} \epsilon_{\omega}^2 L \frac{\sin(\Delta k L/2)}{(\Delta k L/2)} \exp(i\Delta k L/2). \quad (12)$$

For plane waves, the fundamental and harmonic waves must have parallel k vectors, so tilting the waves away from the phase-matching angle by θ introduces the phase mismatch $\Delta k = (k_3\rho_3 - k_2\rho_2 - k_1\rho_1)\theta$. We define the plane-wave acceptance angle (FWHM irradiance) as twice the angle at which the harmonic irradiance falls to half its phase-matched value,

$$\Delta\theta_{pw} = \frac{0.866(2\pi)}{L(k_3\rho_3 - k_2\rho_2 - k_1\rho_1)}. \quad (13)$$

In two walk-off-compensating crystals of length $L/2$, adjusted so $\Delta k_a = \Delta k_b = 0$ for an untilted fundamental wave, a tilt of θ will induce the phase mismatches $\Delta k_a = -\Delta k_b = k_{2\omega}\rho\theta$ for type I mixing or $\Delta k_a = -\Delta k_b = (k_{2\omega} - k_{\omega})\rho\theta$ for type II mixing. The harmonic field radiated by the first crystal, including the phase shifts $\Delta k_a L/2$ and $\Delta k_b L/2$, which are due to linear propagation through the first and second crystals, is

$$\begin{aligned} \epsilon_{2\omega}^a &= i \frac{\omega d_{\text{eff}}}{nc} \epsilon_{\omega}^2 \frac{L}{2} \frac{\sin(\Delta k L/4)}{(\Delta k L/4)} \exp(i\Delta k L/4) \\ &\quad \times \exp(-i\Delta k L/2), \end{aligned} \quad (14)$$

while the field radiated by the second crystal is

$$\epsilon_{2\omega}^b = i \frac{\omega d_{\text{eff}}}{nc} \epsilon_{\omega}^2 L \frac{\sin(\Delta k L/4)}{(\Delta k L/4)} \exp(-i\Delta k L/4). \quad (15)$$

The coherent sum of these is

$$\begin{aligned} \epsilon_{2\omega} &= \epsilon_{2\omega}^a + \epsilon_{2\omega}^b \\ &= i \frac{\omega d_{\text{eff}}}{nc} \epsilon_{\omega}^2 L \frac{\sin(\Delta k L/4)}{(\Delta k L/4)} \exp(-i\Delta k L/4). \end{aligned} \quad (16)$$

Comparison of Eqs. (12) and (16) shows that the allowable range of Δk , or equivalently, the allowable tilt of the fundamental wave, has increased by a factor of two relative to the single crystal. If we apply the same method to N crystals of length L/N with alternating Δk , we find

$$\epsilon_{2\omega} = i \frac{\omega d_{\text{eff}}}{nc} \epsilon_{\omega}^2 L \frac{\sin(\Delta k L/2N)}{(\Delta k L/2N)} \exp[(-1)^{N+1} i \Delta k L/2N], \quad (17)$$

demonstrating that spatial walk-off compensation increases the plane-wave acceptance angle for N crystals, each of length L/N , to N times that of a single crystal of length L . Furthermore, this solution indicates that, for plane waves, N walk-off-compensating crystals in perfect alignment behave exactly like a single crystal with the same total length but with a walk-off angle N times smaller. Similar considerations show that, for temporal walk-off compensation, the acceptance bandwidth increases by N .

Phasor diagrams conveniently illustrate this plane-wave case. Figure 1 shows a diagram for six walk-off-compensating crystal segments. In the top diagram, $\Delta k = 0$ in all six segments. Arrows 1–6 represent the harmonic-field contributions from the six segments as seen at a detector located beyond the sixth crystal. The phasor length and tilt represent, respectively, the amplitude and phase of the harmonic field. The angle between the head and tail of a phasor is $\Delta k L/6$, where Δk is the phase mismatch for that segment and $L/6$ is the segment length. The harmonic irradiance from the set of crystals is proportional to the square of the length of the resultant vector from the tail of segment 1 to the head of segment 6. The next diagram is the same, but for nonzero Δk , with equal magnitude and alternating sign, as is appropriate for a tilted fundamental wave. As the magnitude of the tilt and thus Δk , increases the curvature of each segment increases, reducing the resultant field in proportion to the shortening of the single-segment resultant field, verifying the notion that the acceptance angle for the array of segments is that of a single segment. If the crystals were arranged without walk-off compensation, Δk would have the same sign in each segment, and the phasors would all curve in the same direction with head-to-tail angle $\Delta k L$.

Phasor diagrams also make it easy to visualize the effect of detuning individual crystal segments, addressing the issue of sensitivity to misalignment of any of the segments. The third phasor diagram in Fig. 1 represents perfect alignment of segments 2–6 but misalignment of segment one, while the bottom diagram is the same except that segment 3 alone is misaligned. It is apparent that misalignment of the middle segments is more detrimental than misalignment of the end crystals, but even

for the middle segments, the angular tolerance is greater than that for a single crystal of length L . This is verified by the curves in Fig. 2, which show the harmonic irradiance from the crystal array as various crystal segments are tilted. The width of the phase-matching curve for segment three is roughly $\Delta k L/6 = \pi$, so its angular tolerance is nearly three times that of a single crystal of length L . More generally, for N segments, the greatest angular sensitivity to misalignment of a single segment is roughly $2/N$ times that of a single crystal of the same overall length.

As a laboratory demonstration of increased plane-wave angular acceptance for walk-off-compensating crystals, we recorded phase-matching curves for type I frequency doubling in four BBO crystals, using the experimental apparatus depicted in Fig. 3. A highly collimated, spatially filtered, 4-mm-diameter beam of 1064-nm light from a single-longitudinal-mode Nd:YAG laser (Continuum NY82-10) passed through four identical 7-mm-long BBO crystals antireflection coated for 1064 and 532 nm. The large beam diameter and the narrow frequency spectrum ensured a good approximation to the plane-wave limit, and the pulse energy was kept low to ensure low-conversion efficiency. The crystals were oriented to have the same sign¹¹ of d_{eff} and individually rotated to the phase-matching angle. Shifts of the relative phase $\phi_{2\omega} - 2\phi_{\omega}$ owing to the 3-mm air gaps between the crystals and the antireflection coatings were negligible. We recorded phase-matching curves by fixing the crystal angles and tilting the fundamental beam by means of a rotating mirror mounted on a galvanometer scanner with 10- μrad resolution. After passing through the crystals, a few per-

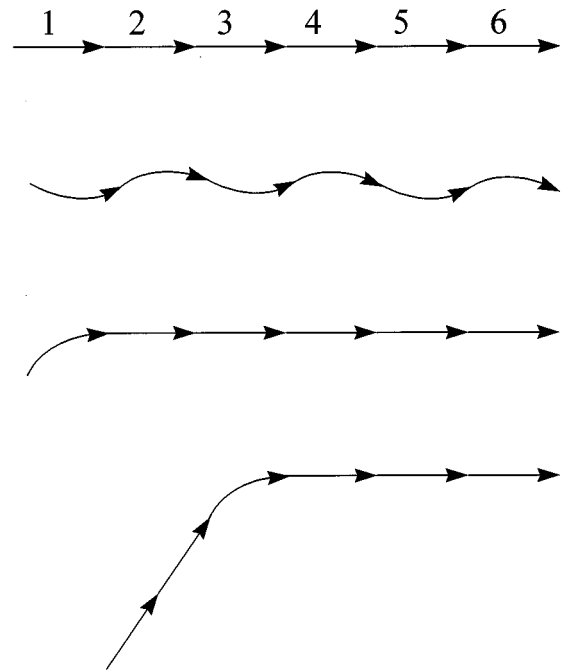


Fig. 1. Phasor diagrams for six walk-off-compensated crystal segments. In the upper diagram, $\Delta k = 0$ for all segments. In the second diagram Δk is equal in magnitude but with alternating sign. In the third diagram, $\Delta k = 0$ for all except the first crystal segment. In the fourth diagram, $\Delta k = 0$ for all except the third crystal segment.

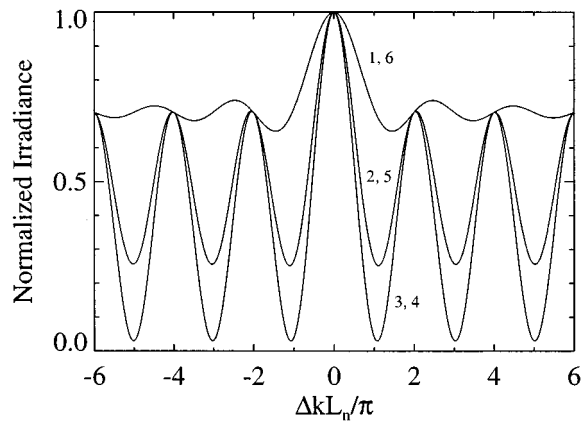


Fig. 2. Effect of detuning one crystal segment of length L_n in an array of six segments. Curve 1,6 shows how low conversion-frequency doubling depends on detuning of segment 1 or segment 6. Similarly, the curves labeled 2,5 and 3,4 show the effect of detuning segments 2 or 5 and segments 3 or 4.

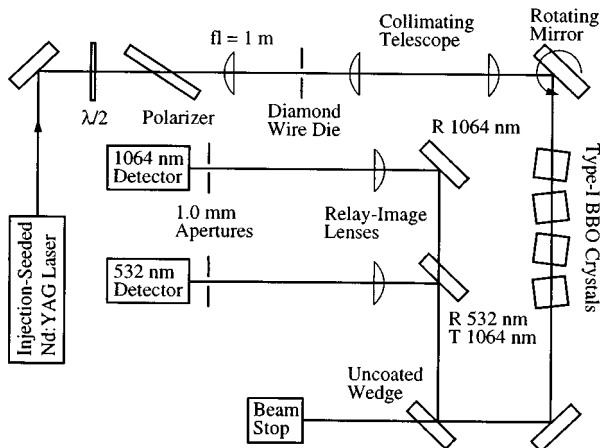


Fig. 3. Apparatus for measuring phase-matching curves with four 7-mm-long BBO crystals by means of an injection-seeded Nd:YAG laser: $\lambda/2$, half-wave plate; R, reflectance; T, transmittance; fl, focal length.

cent of the 532-nm and 1064-nm light was split off by an uncoated wedge and separated into individual beams directed to separate phototubes. Lenses imaged the pivot point of the rotating mirror onto 1-mm-diameter apertures in front of the phototubes so the beams remained centered on the apertures as the mirror tilted. The phototube signals were processed by gated integrators, and average pulse energies versus mirror angle were recorded by a computer-controlled data-acquisition system. Type I doubling of 1064 nm in a single 7-mm-long BBO crystal is expected to have an internal acceptance angle of 0.83 mrad (corresponding to 49-mrad walk-off), and this was verified by data represented by the solid curve in Fig. 4. With four 7-mm-long walk-off-compensating crystals, the acceptance angle was the same, as shown by the circles, whereas four noncompensating crystals had an acceptance angle four times smaller, as shown by the squares, verifying that the acceptance angle for four walk-off-compensating crystal segments is the same as that of the individual segments and four times that of a single crystal of the same net length.

B. Collimated Gaussian Beams

We show in this section how walk-off reduces mixing efficiency as well as the acceptance angle (bandwidth) for collimated Gaussian beams with birefringent (group-velocity) walk-off comparable to the beam diameter (duration) and how walk-off compensation counteracts these reductions. This analysis will be entirely in the local description, but we will demonstrate its equivalence to an analysis in the Fourier description. We will show that the critical factor in determining acceptance angles for collimated beams is not the polarization of the fields but the relative alignment of their Poynting vectors, so, with apologies for introducing more nomenclature, we coin the terms type A and type B mixing to classify two general categories. In type A mixing the two input beams have parallel Poynting vectors, but the product beam walks off from them. In type B mixing the Poynting vectors of the input beams are not parallel, and the Poynting vector of the product beam parallels one of them. Type A includes collinearly phase-matched mixing of two o(e) waves to generate an e(o) wave, while type B includes mixing an e and an o wave to produce an e or an o. More generally, any process can be forced to be either type A or type B by tilting the input beams in the appropriate way. For example, tangentially phase-matched sum-frequency generation in a negative uniaxial crystal uses two o input beams, but one is tilted to propagate parallel to the Poynting vector of the product e wave. This is type B, even though both input beams are o polarized. Similarly, mixing an e and an o wave is type A if the e input beam is tilted so its Poynting vector parallels that of the o input beam. Unfortunately these noncollinearly phase-matched processes cannot be walk-off compensated by means of crystal segments of alternating walk-off direction except for plane waves, but the discussion below otherwise applies to these situations as well as to collinear phase matching. Clearly, there is a range of other possibilities in which no two waves have parallel Poynting vectors, but the two types, A and B, represent important limiting cases.

The corresponding categories for temporal walk-off replace the term Poynting vector with group velocity. In practice, actual cases span the range between type A, for

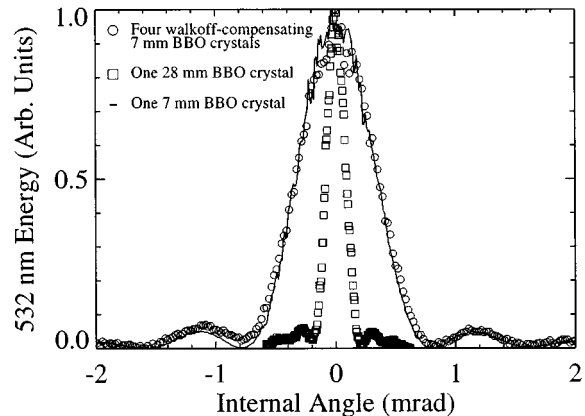


Fig. 4. Low-conversion phase-matching curves recorded with the spatially filtered Nd:YAG laser for one 7-mm BBO crystal, four 7-mm walk-off-compensating crystals, and one 28-mm crystal.

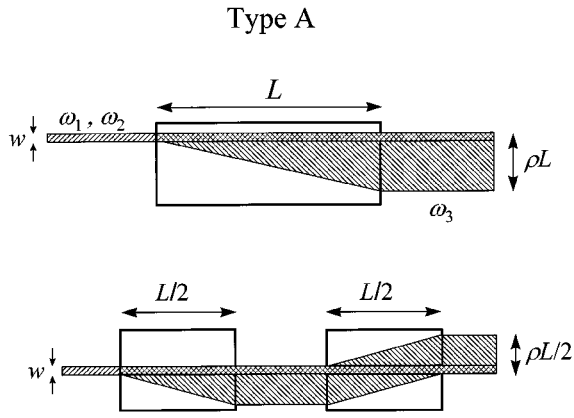


Fig. 5. Beam behavior in a birefringent crystal for type A frequency doubling in a single crystal (upper) and in two walk-off-compensating segments (lower).

which two input pulses stay overlapped but walk off from the product pulse, and type B, for which the product pulse stays overlapped with one of the input pulses.

1. Type A Mixing

As a reminder, in this context collimated Gaussian beams have a Gaussian spatial profile and are weakly focused at the center of the crystal, with a confocal length much greater than the crystal length, implying that the phase fronts are nearly planar throughout the length of the crystal. Figure 5 illustrates spatial walk-off and two-crystal compensation. Consider first the influence of spatial walk-off on single-crystal mixing efficiency for beam diameters comparable to or smaller than the birefringent walk-off, ρL . We assume the input beams have equal widths W in the walk-off direction and heights H in the other transverse direction. Each z slice of the crystal radiates a product field in a Gaussian beam of width W and height H offset in the walk-off direction by $-\rho z$ relative to that radiated by the $z = 0$ slice. The fields from all contributions are equal and combine in perfect phase if $\Delta k = 0$, implying that the area integral of the product field is a constant independent of the product-beam size, and thus independent of walk-off. In contrast, the area integral of the square of the product field, or the product power, is reduced owing to walk-off by the ratio of the actual product-beam size, approximately $(W + \rho L)$, to the beam size without walk-off, W . This reduction is reflected in the following empirical expressions for the mixing efficiency, which we derived by combining standard analytic expressions for mixing efficiency at $\rho = 0$, with the results of modeling a range of ρ 's.²⁰ For type A sum- and difference-frequency mixing of cw Gaussian beams with identical spatial profiles in a single crystal, the product power is given within 2% by

$$P_3 = \frac{(1.31 \times 10^{-2})d_{\text{eff}}^2 P_1 P_2 L^2}{WH\lambda_3^2 n_1 n_2 n_3} \left[\frac{1}{\sqrt{1 + 0.51(\rho L/W)^2}} \right], \quad (18)$$

where the quantity in braces is a walk-off-correction term derived from modeling. For mixing two input beams with identical spatial and temporal Gaussian profiles, the pulse energy is

$$U_3 = \frac{(8.71 \times 10^{-3})d_{\text{eff}}^2 U_1 U_2 L^2}{TWH\lambda_3^2 n_1 n_2 n_3} \left[\frac{1}{\sqrt{1 + 0.51(\rho L/W)^2}} \right]. \quad (19)$$

The subscripts 1 and 2 refer to input light of frequencies ω_1 and ω_2 , and subscript 3 refers to light at the generated frequency $\omega_1 \pm \omega_2$. Units are millimeters for W , H , and L ; seconds for T ; nanometers for vacuum wavelength λ ; watts for P ; joules for U ; and pm/V for d_{eff} . The quantities W , H , and T are FWHM irradiance values for the beam widths and pulse duration. For second-harmonic generation, half the input power or energy should be assigned to P_1 or U_1 and half to P_2 or U_2 . We note that expressions for P_3 in integral form are available in the literature^{21,23} for both type A and type B mixing, but we offer the easily evaluated expressions above as a convenience to the reader.

If the crystal is divided into two walk-off-compensating segments of length $L/2$, as shown in the lower diagram of Fig. 5, the area of the product beam is reduced, and its power is correspondingly increased. It should be evident, based on the product-beam area, that the efficiency can be calculated by replacing ρ in Eqs. (18) and (19) with $\rho/2$. We verified this using our numeric models. More generally, cutting the crystal into N segments reduces the effective walk-off angle by N , improving the conversion efficiency by the amount indicated by Eqs. (18) or (19) with ρ replaced by ρ/N .

Equation (19) is also valid for mixing pulses when temporal walk-off is important but spatial walk-off is negligible, assuming the beams have Gaussian spatial and temporal profiles, and assuming type A mixing where the two input pulses have the same group velocity v_1 . The quantity $\rho L/W$ should be replaced by $\sigma L/T$, where σL is the temporal walk-off between the input and generated pulses that is due to the difference in their group velocities, with σ defined as

$$\sigma = \frac{1}{v_3} - \frac{1}{v_1}. \quad (20)$$

Returning to spatial walk-off, the far-field angular distribution of the generated wave is the Fourier transform of the product field at the crystal exit face. This field extends over a range in the walk-off direction that increases with the walk-off angle, implying that the far-field angular range in the x direction must shrink with increasing walk-off. This shrinkage is a manifestation of the limited acceptance angle of the crystal. Product waves are generated only within the confined range of this acceptance angle. At the exit face the product field comprises the sum of the product fields emitted from each z slice of the crystal. Each slice generates a Gaussian profile beam of width W laterally offset by $-z\rho$ because of spatial walk-off. Applying the convolution theorem for Fourier transforms to the integral over these slices, the angular distribution must be proportional to the product of the transforms of a Gaussian of width W and a step function of width $L\rho$. The power of energy distribution in air is the square of this,

$$P(\theta) \propto \exp\left[\frac{-W2\pi\theta}{\lambda\sqrt{8\ln(0.5)}}\right]^2 \text{sinc}^2(\pi\theta\rho L/\lambda), \quad (21)$$

where λ is the product wavelength in air and θ is measured from the phase-matching angle. The exponential term is a Gaussian of angular width (FWHM),

$$\delta\theta = \frac{0.624\lambda}{W}, \quad (22)$$

while the squared sinc term has a width (FWHM) of

$$\delta\theta = \frac{0.886\lambda}{\rho L}. \quad (23)$$

The far-field angular spread is approximately the lesser of these. If $\rho L \gg W$, the angular spread is given by Eq. (23), and is equal to the plane-wave acceptance angle defined in Eq. (13) multiplied by n to convert from internal to external angle. If N -crystal walk-off compensation is used, ρ is replaced in Eq. (23) by ρ/N , increasing the far-field angular distribution by as much as a factor of N . The angular spread cannot be greater than that given by Eq. (22), however, even when the effective walk-off is much less than W . In other words, the upper limit on the far-field angular spread is that of a product beam of width $W/(2)^{1/2}$, but if walk-off is large, it is reduced to the crystal's acceptance angle.

Similarly, temporal walk-off stretches the product wave in time, implying a restricted spectral bandwidth that is a manifestation of the crystal's limited acceptance bandwidth. An example is shown in Fig. 6 for frequency doubling. The upper plot shows spectra of the fundamental and harmonic pulses, which are Fourier transforms of the time profiles shown in the lower plot. The narrower spectrum and the longer pulse are those of the harmonic. These curves were generated by integrating the mixing equations in a single crystal with the temporal walk-off σL set to 6.7 times the fundamental-pulse duration T . If the walk-off were reduced by a factor of 2, the harmonic-pulse duration would be approximately halved, and the harmonic spectrum would broaden by nearly a factor of 2, almost doubling the conversion efficiency.

It is worth making a distinction between tilt tolerance and acceptance angle. For plane waves, the acceptance angle was the same as the tilt tolerance, but that is not the case for beams of limited extent such as the collimated Gaussian beams under discussion here. The tilt tolerance can be evaluated by considering the effect of tilting the two input beams away from the phase-matching angle. We will use the convention that the phase mismatch is that associated with the carrier, or central, plane waves of the input beams and the product plane wave with a parallel k vector. Using Eq. (10), we see that tilting the input beams by α introduces a phase-velocity mismatch of $2\pi\rho\alpha/\lambda$. The contributions of the various z slices no longer have identical phases, resulting in reduced mixing efficiency because of destructive interference. In a single crystal with large walk-off, destructive interference becomes significant when the phases slip by more than approximately $\pi/2$ over the length of over-

lap between input and product rays, $l = W/\rho$. Using the definition of phase-mismatch tolerance (FWHM),

$$\Delta kl = 0.886 \times 2\pi, \quad (24)$$

we find that the tilt tolerance $\Delta\theta$ is

$$\Delta\theta = 0.886\lambda/W, \quad (25)$$

where λ is the product wavelength. This is approximately the angular range given by Eq. (22) and is the far-field divergence of a product beam of diameter $W/2$. For small walk-off, the tilt tolerance approaches the plane-wave value of Eq. (23), so in general the tilt tolerance is the larger of the angles of Eqs. (22) and (23). Note that segmenting the crystal with walk-off compensation does not increase the tilt tolerance until the acceptance angle overtakes the angular range of the input beams, even though the acceptance angle and mixing efficiency are increasing while $\rho L \gg W$.

Furthermore, in a single crystal, when the input beams are tilted slightly ($\Delta kL \ll 2\pi$) away from the exact phase-matching angle, the product light created near the entrance face and located at the exit face on the edge of the product beam away from the input beams has a phase

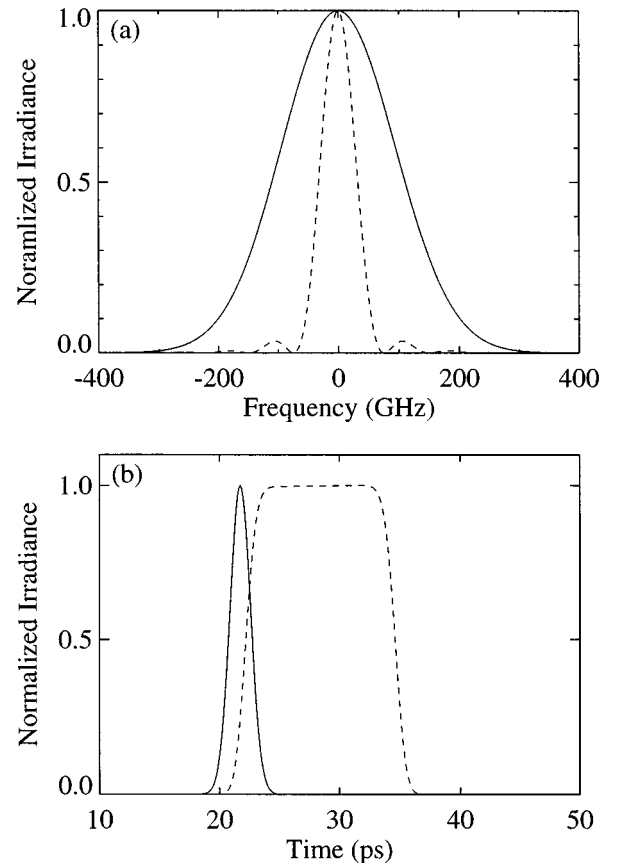


Fig. 6. (a) Fundamental and second-harmonic spectra, and (b) time profiles for type I frequency doubling as calculated by numeric integration of mixing equations ignoring diffraction, birefringent walk-off, and group-velocity dispersion. Group-velocity walk-off stretches the harmonic-pulse duration to ~ 6.7 times that of the fundamental pulse. The spectra are Fourier transforms of the temporal-pulse shapes. Similar angular spectral narrowing is associated with spatial broadening related to birefringent walk-off.

shift relative to that of the light created near the exit face and located on the opposite edge of the product beam. The phase difference, owing to phase-velocity mismatch, tilts the phase front of the product beam toward the phase-matching direction. Consequently, for narrow acceptance angles, the direction of the product beam is nearly fixed relative to the crystal and does not tilt with the input beams.

Note that the reduced efficiency and restricted product bandwidths and far-field angles arise entirely within the local description without directly invoking acceptance angles or bandwidths. Alternatively, we can analyze type A second-harmonic generation entirely in terms of the Fourier description. The plane-wave acceptance angle is defined in terms of tilts of the fundamental and harmonic plane waves away from the phase-matching angle. The refractive index of the harmonic wave changes with tilt at a rate of $dn/d\theta = n\rho$, inducing a phase-velocity mismatch between the fundamental and second-harmonic plane waves. The acceptance angle $\Delta\theta$ (FWHM), defined as the angle at which $\Delta kL = 0.866 \times 2\pi$, is given by

$$\Delta\theta = \frac{0.443\lambda}{L\rho n}, \quad (26)$$

where λ is the vacuum wavelength of the fundamental. This is very nearly the far-field diffraction angle (FWHM) of a fundamental Gaussian beam with focal waist (FWHM diameter) equal to the walk-off, $L\rho$. The harmonic power is the sum of the powers of the individual harmonic plane waves, so the reduction in the number of allowed harmonic plane waves for large ρ 's reduces the harmonic power by $W/\rho L$, the ratio of the plane-wave acceptance angle to the far-field angle of the fundamental. We showed earlier that walk-off compensation in N segments increases the acceptance angle for plane waves by N , so once again ρ should be replaced by ρ/N , thereby improving efficiency. We emphasize that the reduction in efficiency with walk-off is related to the restriction in harmonic angle, not the fundamental angle, and that all Fourier components of the fundamental contribute to harmonic generation if $\Delta k = 0$. Fundamental plane waves tilted in one direction combine with waves tilted in the other, according to the convolution integral of Eq. (6), to produce the harmonic waves. Similarly, for temporal walk-off, the harmonic spectrum is narrowed, but all spectral components of the fundamental still contribute to harmonic generation. The blue components combine with the red as allowed by the convolution integral.

2. Type B Mixing

Figure 7 depicts type B mixing. The upper diagram illustrates how a large walk-off limits the effective interaction length to $l \approx W/\rho$ for two input beams of width W . For type B mixing with collinear input beams of identical Gaussian spatial profiles exactly overlapped at the input face of the crystal, the correction terms in Eqs. (18) and (19) are replaced by $1/[1 + 0.6(\rho L/W)^2 + 1.0(\rho L/W)^4]^{1/2}$ to give the output energy or power within 5%. Higher efficiency is possible by offsetting the input beams so that walk-off causes them to cross midway through each crystal segment rather than at the input face. The coeffi-

cients 0.6 and 1.0 under the radical are then replaced by 0.15 and 0.095, respectively, reflecting an efficiency enhancement greater than three for large walk-off ($\rho L > W$). Still greater mixing efficiency is possible by increasing the width of the beam that walks off to approximately ρL and positioning it to be centered on the other input beam at the crystal center. Modeling indicates that if the beam width (FWHM) is set to the greater of W or $0.6\rho L$, the efficiency is nearly identical to that for type A mixing, and Eqs. (18) and (19) apply, with W or T referring to the smaller input beam. In any of these situations, walk-off compensation in N segments can be accounted for by replacing ρ with ρ/N . For temporal walk-off, the quantity $\rho L/W$ is to be replaced by $\sigma L/T$.

In a single segment, the widths of the two output beams with parallel Poynting vectors are approximately W , implying Fourier transforms or far-field angular distributions unnarrowed by spatial walk-off. The distribution of the third beam is modified in a manner that depends on its width and lateral position at the input face. If it has width W and overlaps the other input beam at the crystal face, the output beam consists of a depleted beam of width W plus a spatial sideband generated by frequency mixing among the other two beams. Likewise, for temporal walk-off, the durations of the two pulses with the same group velocity are approximately those of the input pulses, but the other pulse develops a temporal side lobe. This side lobe is generated only in the region past the overlap zone, so its width depends on the location of the overlap. In sum-frequency mixing, the phase of the side lobe light is opposite that of the input beam, causing a redistribution of energy among the plane waves comprising the ω_1 output beam.

Figure 8 shows the frequency spectrum for second-harmonic generation when the input pulses are exactly overlapped at the input face of a crystal with temporal walk-off. Frequencies near the line center of the ω_1 light are depleted, while the adjacent peaks are boosted. Overall mixing efficiency is decreased by mixing past the overlap zone. The width of the dip is inversely related to the duration of the backconversion side lobe, so it is approximately equal to the plane-wave acceptance bandwidth when the overlap zone is near the input face. If the crossing zone is positioned later in the crystal, the side lobe is of shorter duration, resulting in a broader,

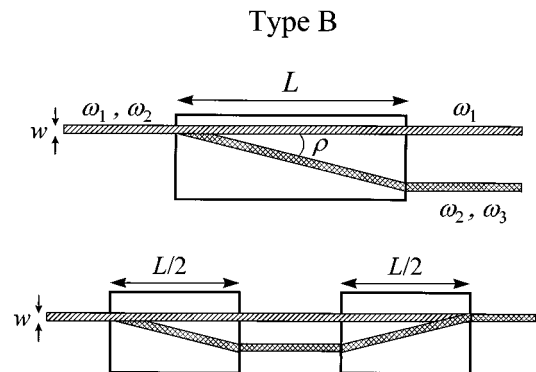


Fig. 7. Beam behavior in a birefringent crystal for type B frequency doubling in a single crystal (upper) and in two walk-off-compensating segments (lower).

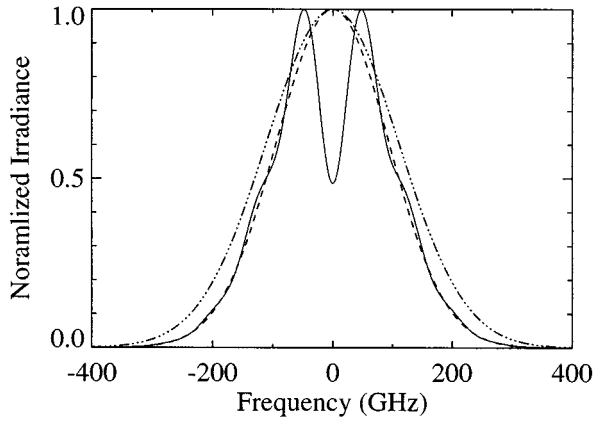


Fig. 8. Spectra for e- and o-polarized fundamental pulses and second-harmonic pulse in type II mixing with group-velocity walk-off $\sigma L = 6.7T$. The o-polarized fundamental spectrum has a dip at the midpoint of the curve, and the second-harmonic spectrum is the broadest.

shallower dip. For a crossing near the exit face, the dip disappears altogether. If the beam with walk-off is adjusted to the optimum duration of $0.6\sigma L$, its output spectrum is nearly the same as the input spectrum. In difference-frequency mixing, the side lobe has the same phase as the main peak if the wave that walks off is the redder of the input beams. The spectral dip is then replaced by a spectral peak of the same width, and mixing efficiency is enhanced by mixing past the overlap zone.

If the input beams are tilted away from the phase-matching direction, the product beam does not tilt, just as for type A. The allowable tilt depends on the effective beam overlap length, l , just as in type A mixing. If the beam with walk-off is broadened to $0.6\rho L$, the overlap length is the full crystal length, and the allowable tilt is reduced to the angular range of the broadened beam, or approximately to the plane-wave acceptance angle.

All of these features of spectral modification can be explained equally well in the Fourier description, of course, but careful attention must be given to the phases of the plane waves to account for the widths and positions of the beams. It is much easier to deduce the behavior in the local picture.

C. Focused Gaussian Beams

We will discuss only type A mixing of focused beams. We consider first spatial walk-off compensation for two crystal segments; then we broaden the discussion to N segments. Boyd and Kleinman²¹ showed that the second-harmonic power for type I doubling a cw Gaussian beam focused at the center of a crystal of length L is

$$P_2 = \frac{5.99 \times 10^4 d_{\text{eff}}^2 P_1^2 L h(\Delta k, B, l, z_0)}{n^2 \lambda_1^3}, \quad (27)$$

where

$$h(\Delta k, B, L, z_0) = \frac{z_0}{2L} \int_{-L/2z_0}^{L/2z_0} \int_{-L/2z_0}^{L/2z_0} d\tau d\tau' \times \frac{\exp[i(z_0 \Delta k)(\tau - \tau') - (2z_0 B^2/L)(\tau - \tau')^2]}{(1 + i\tau)(1 - i\tau')}, \quad (28)$$

$$B = \rho \sqrt{\frac{L \pi n}{2\lambda_1}}. \quad (29)$$

Here λ_1 is the vacuum wavelength of the fundamental, n is the refractive index of the fundamental and the harmonic, and the Rayleigh range is defined by $z_0 = kw_0^2/2$, where w_0 is the beam radius ($1/e^2$ irradiance) at the focus. The value of $h(\Delta k, B, L, z_0)$ and the doubling efficiency are maximized by setting the Rayleigh range and phase mismatch to the values indicated on the graph in Fig. 9. The resulting optimized value of $h(\Delta k, B, L, z_0)$ is that shown in Fig. 9.

Using the methods of Boyd and Kleinman, we find that for two walk-off-compensating crystals, each of length $L/2$, with phase mismatches Δk_1 and Δk_2 , and with a spacing between them much less than z_0 , the function h above is replaced by

$$h(\Delta k_1, \Delta k_2, B, L, z_0) = \frac{z_0}{2L} \int_0^{L/2z_0} \int_0^{L/2z_0} d\tau d\tau' \frac{\exp[-2z_0 B^2/L(\tau - \tau')^2]}{(1 + \tau^2)(1 + \tau'^2)} \times \{ (1 + \tau\tau') \cos[z_0 \Delta k_2(\tau - \tau')] - (\tau - \tau') \sin[z_0 \Delta k_2(\tau - \tau')] + (1 + \tau\tau') \cos[z_0 \Delta k_1(\tau - \tau')] - (\tau - \tau') \sin[z_0 \Delta k_1(\tau - \tau')] \pm 2(1 - \tau\tau') \cos[z_0 \Delta k_1 \tau + z_0 \Delta k_2 \tau'] \mp 2(\tau + \tau') \sin[z_0 \Delta k_1 \tau + z_0 \Delta k_2 \tau'] \}. \quad (30)$$

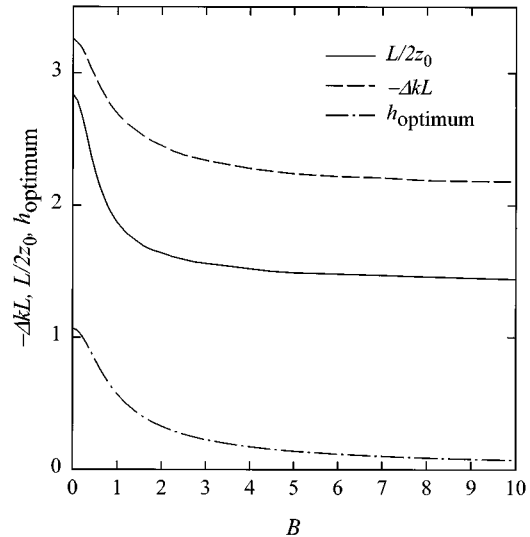


Fig. 9. Optimum values of phase mismatch $-\Delta kL$, focus parameter $L/2z_0$, and $h(\Delta k, B, L, z_0)$ as functions of $B = \rho(L \pi n/2\lambda_1)^{1/2}$.

A similar expression is presented by Zondy.²⁴ The upper (lower) signs on the last two terms are for same (opposite) signs of d_{eff} in the two segments. Similar expressions could be derived for more than two crystal segments, but the number of terms in h would increase rapidly with the number of segments. We numerically evaluated the two-crystal function $h(\Delta k_1, \Delta k_2, B, L, z_0)$ to create the three surfaces of Fig. 10 corresponding to doubling 800-nm light in two 5-mm-long BBO crystals with the same sign of d_{eff} and a walk-off angle of 60 mrad for plane waves [Fig. 10(a)], collimated Gaussian beams [Fig. 10(b)], or focused Gaussian beams [Fig. 10(c)]. If d_{eff} has opposite signs in the two crystal segments, the ridge near the origin of each surface is replaced by a deep valley. For plane waves, we set the beam waist much larger than the walk-off, $\rho L/2$, and chose a Rayleigh range much greater than the crystal length. As we reported earlier,¹¹ we have experimentally verified the shape of this surface. For collimated Gaussian beams we set the walk-off in each segment to three times the 100- μm beam diameter (FWHM), corresponding to a Rayleigh range of 47 mm. For focused beams the walk-off is again 300 μm but the Rayleigh range is set to 3.6 mm. This is the optimum focusing for a single crystal, assuming the walk-off angle ρ should be replaced by $\rho/2$, which results in an effective value of B half that of a single crystal. This procedure may not yield the maximum conversion efficiency, but we believe it gives nearly the optimal value. We have not systematically sought the optimum focus for two crystals.

The surface ridges far from the origin in Fig. 10 correspond to conversion in only one of the crystal segments with little contribution from the other. Tilting a single segment is equivalent to moving along a line parallel to one of the axes so the width of the ridge is a measure of the tilt tolerance for the contributing segment. If the beam waist is made small compared with walk-off, the ridges broaden approximately in accordance with Eq. (25), reflecting the reduction in overlap length between the fundamental and the harmonic waves. This broadening with decreasing beam size is evident in going from Fig. 10(a) to Fig. 10(c). The maximum value of h lies at the origin for plane waves and collimated beams and moves to slightly negative values of Δk_1 and Δk_2 for tight focusing to accommodate the phase shifts associated with focusing. Tilts of the fundamental beam in the critical plane correspond to movement along a diagonal defined by $\Delta k_1 + \Delta k_2 = \text{const.}$, parallel to the ridge near the origin. Clearly, at h_{max} , the tilt tolerance for the fundamental is approximately that of a single segment and increases with tighter focusing. Tolerance of the misalignment of one of the segments at h_{max} , however, is more or less independent of focusing and is approximately $\theta = \pi/k_1\rho L$.

Comparing computed values of h_{max} for optimized focusing in a single crystal with those for two walk-off-compensating segments of the same total length, we find that the efficiency is approximately twice as high for the latter, assuming the walk-off, ρL , is large compared with the beam waist. We verified this by comparing doubling efficiency in pairs of crystals of lithium iodate, BBO, and lithium triborate, with and without walk-off compensation. The power and position of the focusing lens and the

crystal angle(s) were adjusted to maximize the harmonic power in each case. We generated the cw, 806-nm fundamental light by using an external-cavity diode laser coupled to a tapered waveguide amplifier. The external-cavity laser consisted of an SDL 5412 single-mode diode, a collimating lens, and an 1800-lines/nm holographic grating used in a Littrow configuration. The waveguide laser was an SDL 8630 diode laser modified to act as an amplifier. The fundamental light was spatially filtered and collimated to give a 600-mW beam with a smooth, nearly Gaussian spatial profile. We separated the 403-nm second-harmonic light from the fundamental using a dichroic mirror and a colored glass filter and measured the fundamental and harmonic powers with a pho-

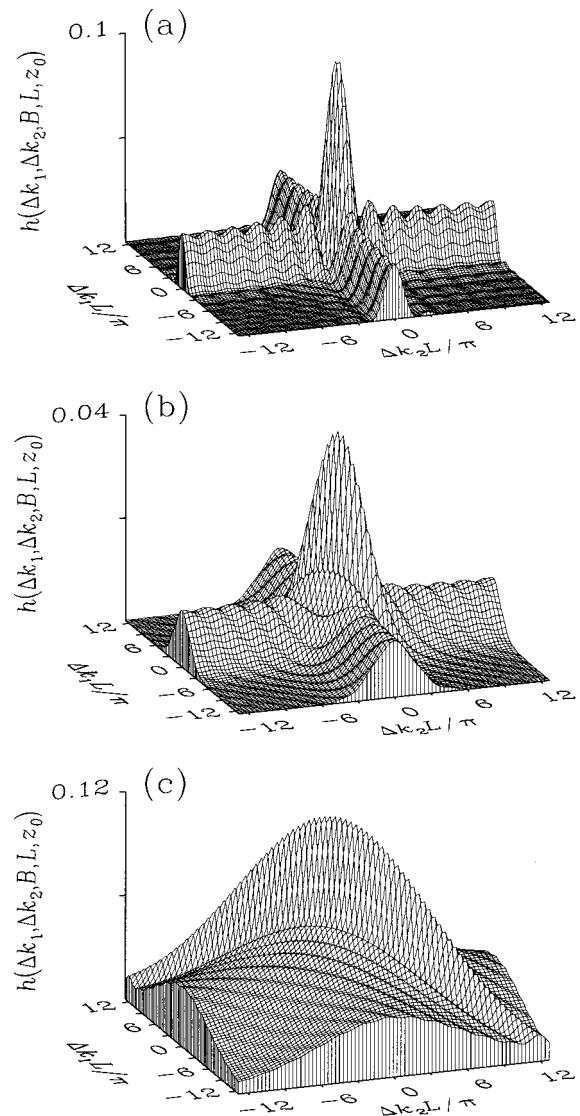


Fig. 10. $h(\Delta k_1, \Delta k_2, B, L, z_0)$ dependence on $(\Delta k_1, \Delta k_2)$ for frequency-doubling 800-nm light in two 5-mm-long crystal segments with 60-mrad walk-off. (a) For plane waves the beam waist is much larger than $\rho L/2$, and the Rayleigh range is much greater than L . (b) For collimated Gaussian beams the walk-off in each segment, $\rho L/2$, is three times the beam diameter of 100 μm (FWHM), and the Rayleigh range is 47 mm. (c) For a focused Gaussian the walk-off $\rho L/2$ is 300 μm , and the Rayleigh range is 3.6 mm.

todiode powermeter (Ophir PD-300-UV). There are four orientations of the second crystal relative to the first that share the critical plane. Conversion efficiency is optimized only if the signs of d_{eff} are the same in the two crystals,¹¹ and the walk-off directions are opposite. When optimized, this arrangement produces about twice the harmonic power of the other three orientations, providing a useful signature of proper crystal orientation. It is also important to position the crystal segments as closely together as possible to achieve the full benefit of walk-off compensation because the focal region centered at the midpoint accounts for a large part of the harmonic generation. We measured $67 \mu\text{W}$ of harmonic light with two 10-mm-long segments of lithium iodate without walk-off compensation and $114 \mu\text{W}$ with compensation. The comparable values for 10-mm segments of lithium triborate are 19 and $34 \mu\text{W}$, while for 5.1-mm segments of BBO they are 17 and $27 \mu\text{W}$. The enhancements that are due to walk-off compensation are 1.7 in lithium iodate, 1.8 in lithium triborate, and 1.6 in BBO. These results are in good agreement with Eqs. (27)–(30) when reflective losses at the crystal surfaces are taken into consideration.

Turning to walk-off compensation in N segments of length L/N , recall that for both plane waves and collimated Gaussian beams, walk-off compensation in N segments can be accounted for quantitatively by replacing ρ by ρ/N in the expressions for conversion efficiency and acceptance angle. If this substitution worked for focused beams, the value of B in Eqs. (27)–(29) would be replaced by $B_{\text{eff}} = B/N$ to predict the performance of walk-off compensation. However, it is not exact for beams with non-planar wave fronts because walk-off causes a dephasing between the fundamental and the harmonic waves. Nevertheless, it might be a reasonable approximation at the optimum phase mismatch, where the overall phase shift between the two waves is minimized. We tested this notion by using both calculations and laboratory measurements. The calculations were numeric integrations of the mixing equations, ignoring group velocity and group-velocity dispersion, but including diffraction and spatial walk-off. The results are shown in Fig. 11. The solid curve represents optimized second-harmonic generation according to the formulas of Boyd and Kleinman²¹ for a single crystal of length L for a range of values of B . The filled squares are data calculated for a crystal with $B = 4$ divided into 1, 2, 3, 4, 8, or 60 segments. The efficiency is calculated with the optimal focus for a single crystal of length L and $B = B_{\text{eff}} = 4/N$ and plotted versus B_{eff} . The data represented by open circles are the same for a crystal with $B = 8$ divided into 2, 4, 6, 8, or 16 segments. We conclude that replacing ρ with ρ/N in the single-crystal expressions and optimizing the focus for B_{eff} works quite well as a rule of thumb for predicting the performance of N walk-off-compensating segments. If the rule were exact, the symbols of Fig. 11 would lie on the solid curve.

As an experimental test of this prediction, we compared doubling efficiency for a single 28-mm BBO crystal with that for four 7-mm BBO segments arranged to compensate walk-off with essentially the same experimental setup as shown in Fig. 3. The antireflection-coated crystal segments were mounted on picomotor-controlled mir-

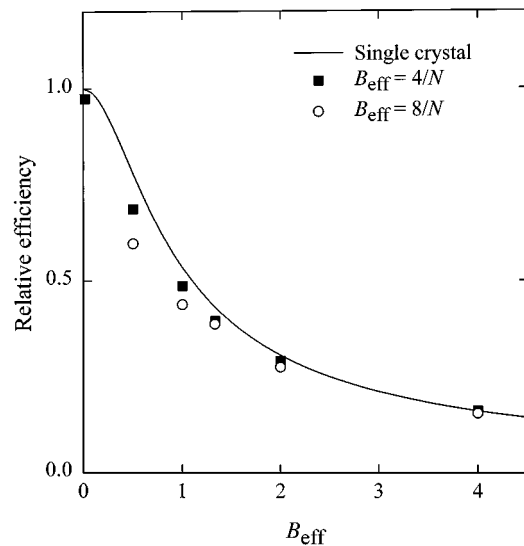


Fig. 11. Comparison of calculated second-harmonic-generation efficiency versus B_{eff} for a single crystal, for 1, 2, 3, 4, 8, or 10 walk-off-compensating segments of a crystal with $B_0 = 4$, and for 2, 4, 6, 8, or 16 walk-off-compensating segments of a crystal with $B_0 = 8$.

ror mounts, and the laser beam was reflected through the crystals by the rotating mirror mounted on a galvanometer scanner. The pulsed Nd:YAG laser was replaced by a 5-mW single-longitudinal-mode Nd:YAG laser (Lightwave Electronics Model 120). A Newtonian telescope focused the 1064-nm light through the crystals with a far-field divergence of 8.5 mrad (FWHM). The positions of the lenses were adjusted to optimize the second-harmonic efficiency while keeping the focus at the midpoint of the crystal array. The 532-nm harmonic light was detected with a Hamamatsu P2368 photomultiplier behind an opal glass diffuser and an interference filter. The crystals were first arranged with a common walk-off direction, then with an alternating walk-off direction, and they were carefully adjusted each time for maximum harmonic power. Repeated measurements alternating between crystal orientations demonstrated an enhancement of 3.3 attributable to walk-off compensation, in good agreement with an enhancement of 3.4 calculated by numeric integration of the mixing equations.

Finally, we note that the spatial profile of the harmonic beam is substantially modified by the use of walk-off compensation. The harmonic profile from a single crystal resembles a Gaussian elongated in the walk-off direction. When N walk-off-compensating crystals are used, the profile is compressed by approximately N in the walk-off direction, and tends toward a flat topped rather than a Gaussian profile.

D. Structured Beams

Exact calculations of parametric mixing with poor quality beams such as those sometimes produced by high-Fresnel-number optical parametric oscillators or dye lasers requires a complete description of the beam, but some general properties may be inferred for beams with a large number of modes with random phase and amplitude. Such beams usually have well-developed speckle

patterns with irradiance distributions²⁵ obeying $P(I) = \exp(-II_0)$, where I_0 is the average irradiance and $P(I)$ is the probability that the irradiance at any particular point is I . It is well known that for zero walk-off this speckle leads to a factor of 2 enhancement in doubling efficiency compared with a smooth profile beam of the same overall shape, size, and power.²⁶ The factor of 2 falls to unity for general sum- and difference-frequency mixing when the speckle patterns of two input beams are uncorrelated. The enhancement of a factor of 2 applies for either spatial and temporal speckle. If spatial walk-off becomes comparable to the spatial speckle size, or if temporal walk-off becomes comparable to the temporal speckle or fluctuation time, the conversion efficiency usually is diminished. We consider two particular cases below.

1. Type A Mixing

An input beam that is M times diffraction limited has an angular spectrum roughly M times as broad as that of a single-mode beam, so there are approximately M speckles distributed over the beam width W . If these speckles are large enough that diffraction over the length of the crystal is unimportant, the speckle pattern propagates relatively unchanged through the crystal. If the spatial walk-off is large compared with the speckle size, the product beam shifts laterally by several speckles relative to the input beams. Because the speckles have random phases relative to one another, the product field along a ray parallel to its Poynting vector is the incoherent sum of contributions from many speckles. The overlap length between the ray and one input-beam speckle is approximately $l = W/M\rho$, and the number of speckles a product ray crosses is $S = M\rho L/W$. The average irradiances of a speckle of the input beams are P_1/WH and P_2/WH , so the power of the product scales approximately as

$$P_3 \propto \frac{P_1 P_2 l^2 S H (\rho L + W)}{H^2 W^2} = \frac{P_1 P_2 L (\rho L + W)}{H W M \rho}, \quad (31)$$

Adjacent product rays cross almost the same set of speckles, so the phase and amplitude structure of the product wave has a scale larger than that of the input beams by approximately S , the number of speckles crossed. In other words, its k_x spectrum is narrowed relative to that of the input beams by S , resulting in a beam quality factor of roughly M/S rather than M . The reduction in product power associated with this spectral narrowing is just that of Eq. (31). The beam quality in the noncritical plane is not changed by the mixing process.

When two walk-off-compensating crystals of length $L/2$ are used, the harmonic field generated in the second crystal is coherent with that generated in the first assuming the speckle patterns of the input beams are the same in the two segments. Consequently the product power is up to four times that generated in one segment of length $L/2$, or twice that generated in a crystal of length L . Similar to the cases discussed above, walk-off compensation in N segments is approximately equivalent to replacing ρ in Eq. (31) with ρ/N .

Similar arguments can be applied to broad bandwidth fields when temporal rather than spatial walk-off is significant. For negligible walkoff, such multimode fields double with twice the efficiency of single-mode fields. As temporal walk-off becomes comparable to or larger than the duration of the temporal speckle irradiance spikes, the doubling efficiency scales as

$$U_3 \propto \frac{U_1 U_2 L (\sigma\tau + T)}{H W T M \sigma}, \quad (32)$$

where M is now the ratio of the bandwidth to the transform-limited bandwidth of the input pulses.

We tested these predictions in the laboratory by doubling a highly structured beam of broad-bandwidth 1064-nm light from a high-Fresnel-number optical parametric oscillator, (Continuum Surelite) pumped by 355-nm light from a Continuum Surelite-II multilongitudinal-mode Nd:YAG laser. The experimental apparatus is diagrammed in Fig. 12. We used the same set of four 7-mm-long type I BBO crystals described above. The diameter of the 1064-nm beam was 2–3 mm, the pulse length ~ 4 ns, and the pulse energy several millijoules. Beam divergence is determined from the phase-matching tilt tolerance shown in Fig. 13 to be ~ 3 mrad, which is ten times the diffractive limit and implies roughly ten speckles across the beam. The average speckle diameter of $\sim 250 \mu\text{m}$ is less than the $350\text{-}\mu\text{m}$ walk-off each 7-mm crystal segment. We relay imaged the output mirror of the optical parametric oscillator onto the BBO crystals with a magnification of 1. As before, the 1064-nm beam was tilted by means of a mirror mounted on a galvanometer, and we compared the phase-matching curves and doubling efficiency for one crystal segment with those for four segments. We recorded the full beam-pulse energy for both the 1064-nm and 532-nm beams and found a 1064-nm depletion of $\sim 1\%$ for a single-crystal segment compared with $\sim 15\%$ depletion for four walk-off-compensating segments, as shown in Fig. 13. With four segments, the total crystal length is increased by a factor of 4, while walk-off compensation reduces the effective walk-off angle by a factor of 4. Ac-

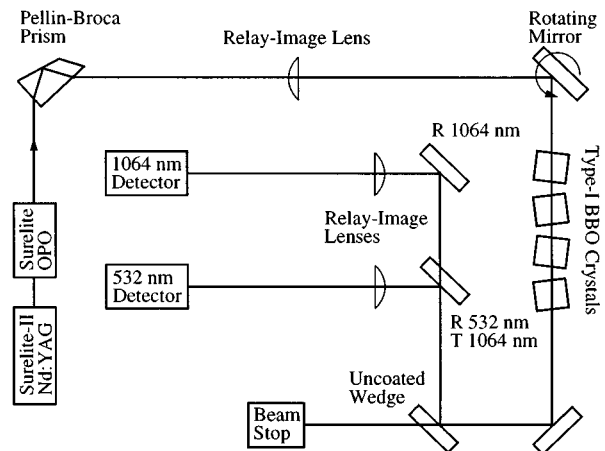


Fig. 12. Apparatus for measuring phase-matching curves for frequency-doubling 1064-nm light from a short-cavity optical parametric oscillator in four 7-mm-long BBO crystals; R, reflectance; T, transmittance.

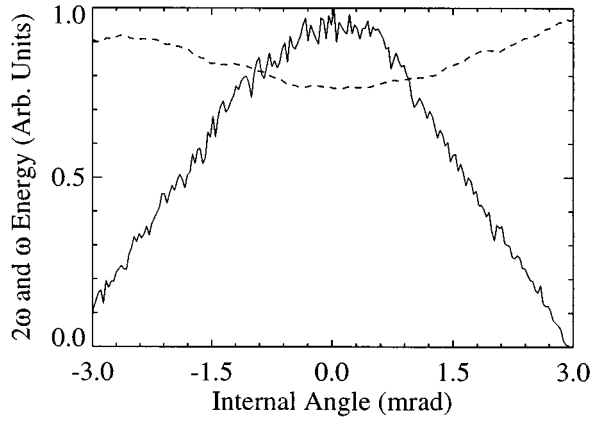


Fig. 13. Doubling signal (solid curve) and 1064-nm pulse depletion (dashed curve) for four walk-off-compensating 7-mm-long crystals.

According to Eq. (31) this should lead to an improvement of a factor of 16 in doubling efficiency, in agreement with our measurements. We did not measure the doubling efficiency for four crystals of the same walk-off direction, but we expect it to be four times that of a single crystal rather than sixteen times as for walk-off-compensated crystals.

2. Type B Mixing

In type B mixing the product field crosses only one of the input beams. The field of the input beam that is parallel to the product beam is constant for a particular ray, while the field of the other beam fluctuates as the ray crosses its speckles. The product power is thus the incoherent sum over speckles, scaling approximately as

$$P_3 \propto \frac{P_1 P_2 L}{H \rho M}, \quad (33)$$

where M is the quality factor for the nonparallel input beam.

With walk-off compensation in two crystals, the effective overlap length of the product ray with the nonparallel input beam is doubled, quadrupling the irradiance generated by each speckle of the input beam. The number of such speckles contributing to each product ray is halved, however, which implies that the incoherent sum of contributions to the product beam is doubled. In general, walk-off compensation in N segments increases the product power by N as long as walk-off in each segment is large compared with the speckle size. If the input beam that walks off is single mode, then there is no benefit from walk-off compensation unless walk-off is comparable to or larger than the beam diameter W , in which case the discussion of collimated Gaussian beams is relevant.

4. PARAMETRIC GAIN WITH LOW PUMP DEPLETION

This section covers three-wave parametric mixing in which the bluest, or pump, input wave is much stronger than the other input wave, which we designate the signal. The signal wave and the third wave, the idler, are amplified at the expense of the pump. We will assume that the

pump wave is not significantly depleted but, in contrast to the previous discussions, we allow large amplifications of the signal.

A. Plane Waves

The well-known plane-wave solution to the mixing equations²⁷ in the limit of low pump depletion can be written

$$\begin{aligned} \epsilon_s(z) = & \epsilon_s(0) \left(\cosh \gamma z - \frac{i \Delta k}{2 \gamma} \sinh \gamma z \right) \exp\left(\frac{i \Delta k z}{2}\right) \\ & + i \frac{A}{\gamma} \epsilon_i^*(0) \sinh \gamma z \exp\left(\frac{i \Delta k z}{2}\right), \end{aligned} \quad (34)$$

$$\begin{aligned} \epsilon_i^*(z) = & \epsilon_i^*(0) \left(\cosh \gamma z + \frac{i \Delta k}{2 \gamma} \sinh \gamma z \right) \exp\left(\frac{-i \Delta k z}{2}\right) \\ & - i \frac{B}{\gamma} \epsilon_s(0) \sinh \gamma z \exp\left(\frac{-i \Delta k z}{2}\right), \end{aligned} \quad (35)$$

where A , B , and γ are constant defined as

$$A = \frac{d_{\text{eff}} \omega_s \epsilon_p}{c n_s}, \quad (36)$$

$$B = \frac{d_{\text{eff}} \omega_i \epsilon_p^*}{c n_i}, \quad (37)$$

$$\gamma = \frac{1}{2} \sqrt{4AB - \Delta k^2}. \quad (38)$$

The subscripts s , i , and p refer to the signal, idler, and pump waves. When $\epsilon_i(0) = 0$, $\Delta k = 0$, and $\gamma \gg 1$, the signal and idler experience exponential gain with an exponent of

$$\gamma L = \left(\frac{2 d_{\text{eff}}^2 \omega_s \omega_i I_p}{\epsilon_0 c^3 n_s n_i n_p} \right)^{1/2} L, \quad (39)$$

or, in practical units,

$$\gamma L = 0.172 d_{\text{eff}} L \left(\frac{I_p}{\lambda_s \lambda_i n_s n_i n_p} \right)^{1/2} \quad (40)$$

where d_{eff} is measured in picometers per volt, I_p is in watts per square centimeter, L is in centimeters, and the vacuum wavelengths λ are in nanometers.

Equations (34) and (35) can be used to predict the behavior of walk-off-compensating crystal segments in the plane-wave limit by use of the output of one segment as the input for the next after adding the phase shifts that are due to propagation, as discussed earlier. Results of such a calculation are presented in Fig. 14, where we show the influence of spatial walk-off compensation on the tolerance to Δk , or beam tilt, for plane-wave parametric gain in 1, 2, or 4 walk-off-compensating segments. Tilting the input beams introduces a Δk of equal magnitude but opposite sign in alternate crystal segments. Defining gain as $(|\epsilon_s(L)/\epsilon_s(0)|^2 - 1)$, we find, as expected, that at low gain, corresponding to the low-conversion difference-frequency mixing discussed above, the acceptance angle is broadened by a factor equal to the number of crystal segments. At higher parametric gains the Δk tolerance for a single crystal increases because nonlinear

coupling among the waves tends to adjust their relative phases to maintain maximal gain. At sufficiently high gain, the phase-readjustment length becomes short compared with the crystal length, so even the segmented crystal perform much like a single crystal, as shown in Fig. 14. These effects were discussed in more detail for two walk-off-compensating crystals in an earlier paper.¹¹

B. Collimated Gaussian Beams and Gaussian Pulses

It is not possible to give simple analytic expressions for parametric gain of collimated Gaussian beams. However, Dou *et al.*²⁸ analyzed parametric gain for collimated beams with spatial walk-off in a single crystal and derived integral expressions for gain that can be numerically evaluated. We present here a discussion of qualitative behavior for N crystal segments inferred from modeling a variety of cases with our computer models. Because one of the input waves is modified by mixing, the type A and B categories above are not inclusive. Instead we must consider the three cases in which either the pump, signal, or idler beam walks off from the other two. At high gain, the signal and idler designations are nearly interchangeable, so we will consider only the first two, referring to them as the pump walk-off and signal-idler walk-off cases.

1. Parametric Gain with Pump Walk-Off

Assuming the input signal and pump beams have widths W_s and W_p , with the Poynting vector of the pump beam tilted by ρ relative to those of the signal and idler beams, the gain length is limited by beam overlap to $l = W_p/\rho$, limiting the gain exponent to $l\gamma$. For walk-offs ρL , large compared with W_p and W_s , the gain is maximized by offsetting the signal wave in the walk-off direction so that all portions of it cross the full pump beam. Then the signal beam retains a width of W_s and generates an idler wave of the same width, so there is no gain narrowing in the walk-off direction. There will be gain narrowing in the other transverse dimension leading to broadening of the far-field angle perpendicular to walk-off. Assuming beam heights of H for the pump and signal beams, this amounts to a broadening of less than a factor of 3 for gain

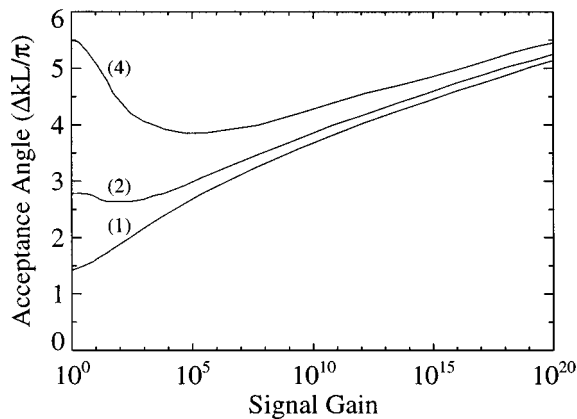


Fig. 14. Angular acceptance, defined as the value of $\Delta kL/\pi$ at which parametric gain is reduced by half, versus parametric gain for a crystal of length L divided into 1, 2, or 4 walk-off-compensating segments.

exponents up to 25, the highest of practical interest. For temporal walk-off, there will likewise be no gain narrowing of the pulse duration. As we discussed for type B mixing above, the full angular and frequency spectra of the pump contribute to nonlinear mixing and drive the parametric gain, but backconversion redistributes the pump spectra slightly in a manner that depends on the location in the crystal of the zone of overlap between the signal and pump beams.

Another similarity to type B mixing above is that spatially broadening the pump beam to ρL while keeping the same height H increases parametric gain. The gain exponent, proportional to $l(I_p)^{1/2}$ will be increased by approximately the factor $(\rho L/W_p)^{1/2}$. Gain is more effectively increased by dividing the crystal into N walk-off-compensating segments, causing the signal and idler beams to cross the pump beam N times. This increases the gain exponent by up to a factor of N . Obviously the gain enhancement can be enormous if the gain per segment is large. Additionally, we verified by modeling that the effect of walk-off compensation in N segments can be exactly accounted for by substituting ρ/N in place of ρ in calculating parametric gain or beam profiles.

2. Parametric Gain with Signal-Idler Walk-Off

Modeling calculations indicate that idler walk-off is more efficient than signal walk-off. The difference is relatively small, however, and decreases with increasing gain, so we do not distinguish between these cases. We will assume for simplicity that the idler walks off. Mixing proceeds throughout the length of the crystal because there is always overlap of the pump with the signal beam. At low gain, the output idler beam has a nearly flat-topped profile in the walk-off direction with a width of approximately ρL , restricting its far-field angular range to the crystal acceptance angle just as in type A mixing above. The full angular spectra of the signal and pump beams participate in mixing. At intermediate parametric gain, the idler wave assumes a nearly exponential profile in the walk-off direction, with the light generated near the exit face exponentially stronger than that generated near the input face. Its far-field angular distribution becomes nearly Lorentzian with a width proportional to the gain exponent of the signal beam. At high gains, where the gain length is less than the walk-off length, the spatial profiles of the signal and idler beams assume nearly identical widths and far-field distributions, with both far-field patterns broadened somewhat relative to the input signal beam owing to spatial gain narrowing.

Walk-off compensation in N segments increases the parametric gain by recycling the idler beam through the pump and signal volume. In the limit of low gain the angular range of the idler increases by N as does the mixing efficiency. At high gain, however, the benefit diminishes. We conclude, based on a limited number of model runs, that at high gain it is the gain rather than the gain exponent that increases by approximately N . The far-field angles are not significantly altered by walk-off compensation. Walk-off compensation is not equivalent to replacing ρ with ρ/N for high gain.

Comparing pump walk-off with signal-idler walk-off, modeling parametric gain in a single crystal indicates

that the overall parametric gain is nearly the same for the two cases if the walk-off ρL is less than or equal to the pump beam width W_p . For larger walk-offs, the signal–idler walk-off geometry has higher gain than the pump walk-off for a given value of ρ . However, the gain improvements available in the latter by broadening the pump beam or using N -crystal walk-off compensation enhances its attractiveness. For quantitative comparison of the two mixing geometries, numerical models are essential. Finally, we note that the narrowing of the plane-wave acceptance angle at moderate gains, seen in Fig. 14 for walk-off compensation, does not imply a reduced acceptance angle for phase-matched parametric gain for collimated Gaussian beams. The narrowing is reflected in increased sensitivity of parametric gain to phase mismatch of the carrier waves but not to a restriction on the angular range of the amplified waves.

C. Structured Beams

One application of parametric gain involving structured beams is amplification of images borne on the signal wave. Fidelity of the amplified image is higher in the pump walk-off geometry because the signal and idler wave copropagate, whereas in the signal–idler walk-off geometry the walk-off between the signal and idler beams causes cross talk between image elements. Another requirement for image fidelity is that the signal and idler beams diffract little over the length of the mixing crystal because they may diffract differently owing to the phase-conjugate nature of the idler and also because the signal and idler may have different wavelengths. In one implementation of image amplification, an image is impressed on a collimated signal beam that is then focused into the mixing crystal. The diffraction length is the confocal length of the full beam divided by the square of the number of resolution elements across the beam. For a signal beam of diameter D with R resolution elements and a lens of focal length F , the spot size at the transform plane of the lens is proportional to $R\lambda F/D$, and the diffractive length is proportional to $n\lambda F^2/D^2 R^2$. If a pump beam of power P_p is adjusted to cover the image-bearing signal beam at the crystal and the crystal length is the diffractive length, the parametric gain exponent is proportional to $(d_{\text{eff}}F/R^3D)(P_p\omega_s\omega_i/n)^{1/2}$ in the absence of walk-off. Because the gain exponent is proportional to F , long focal lengths and long crystals are favored. However, spatial walk-off ultimately limits L and F if ρ is nonzero. The diffraction length and thus the permissible crystal length scales as F^2 while the spot size scales as F , so by limiting the crystal length to that for which pump walk-off equals the signal spot size, $L = R\lambda F/\rho D$, the gain exponent scales as $(d_{\text{eff}}/\rho)(P_p\omega_s\omega_i/n^3)^{1/2}$, indicating that the achievable gain is limited by spatial walk-off. We argued earlier that using N walk-off-compensating crystal segments is equivalent to replacing ρ by ρ/N for pump walk-off, so image-preserving parametric gain can be greatly increased by incorporating walk-off compensation. If temporal walk-off limits the crystal length to T/σ , the gain scales as $(d_{\text{eff}}/R^2)(TP_p\omega_s^2\omega_i/\sigma n^2)^{1/2}$. Decreasing σ by temporal walk-off compensation increases the gain, although less effectively than decreasing spatial walk-off.

5. HIGH-CONVERSION-EFFICIENCY SUM-FREQUENCY MIXING

The assumption that the input waves are unaltered by mixing is obviously no longer valid in high-conversion mixing, so the conclusions of the first part of this paper must be reexamined. Strongly driven sum- and difference-frequency mixing must be discussed separately because they behave quite differently, in contrast to the weakly driven case. The sum-frequency-mixing process $\omega_1 + \omega_2 \rightarrow \omega_3$ is parametrically stable if the input beams are always photon balanced and if the phase mismatch is zero. That is, the reverse process, $\omega_3 \rightarrow \omega_1 + \omega_2$, is avoided. However, difference-frequency mixing is never parametrically stable because the redder input beam grows at the expense of the bluer, eventually depletes the blue wave, and allows the reverse process of sum-frequency mixing. This section is dedicated to studies of sum-frequency generation where the goal is high-conversion efficiency. We pay particular attention to type I doubling because the requirement of photon balance is automatically achieved, and we can concentrate on the influence of phase mismatch and walk-off compensation. General analytic expressions for high-efficiency mixing are not usually available, so we base our discussion largely on numeric integration of the mixing equations similar to those described in Smith and Bowers¹⁹ or Eimerl *et al.*¹⁸ for spatial walk-off and in Sidick *et al.*²⁹ for temporal walk-off.

A. Plane Waves

Figure 15(a) shows a plot of type I doubling efficiency as a function of the fundamental irradiance, I_ω and the phase mismatch ΔkL . We generated it by numerically integrating the mixing equations with parameters appropriate for doubling a 1064-nm, cw plane wave in a single 28-mm-long BBO crystal. The plot shows the well-known narrowing in the ΔkL direction at high irradiance,^{5,30} indicating that the phase velocity of the fundamental wave must be more closely matched to that of the second harmonic at high nonlinear drive than at low. If the phase $\phi_{2\omega} - 2\phi_\omega$ slips by more than approximately $\pi/2$ in passing through the crystal at low drive, the mixing will reverse, converting harmonic light back to fundamental near the exit face of the crystal. The threshold phase shift for this backconversion is reduced as the fundamental irradiance increases because the relative phases of the fundamental and harmonic waves are shifted by nonlinear coupling to favor backconversion rather than frequency doubling. This effect is more pronounced for stronger nonlinear coupling.

This narrowing is an important issue in sum-frequency mixing of real beams because the high irradiance parts of the beam must be overdriven if the lower irradiance parts of the beam are to be efficiently converted. For example, in a pulse that is Gaussian in space and time, 25% of the energy arrives at irradiance levels less than one eighth the maximum irradiance, so conversion efficiencies of 75% or greater require that the maximum irradiance portions be driven approximately 5 to 10 times harder than is necessary for high conversion. The hot spots must be driven

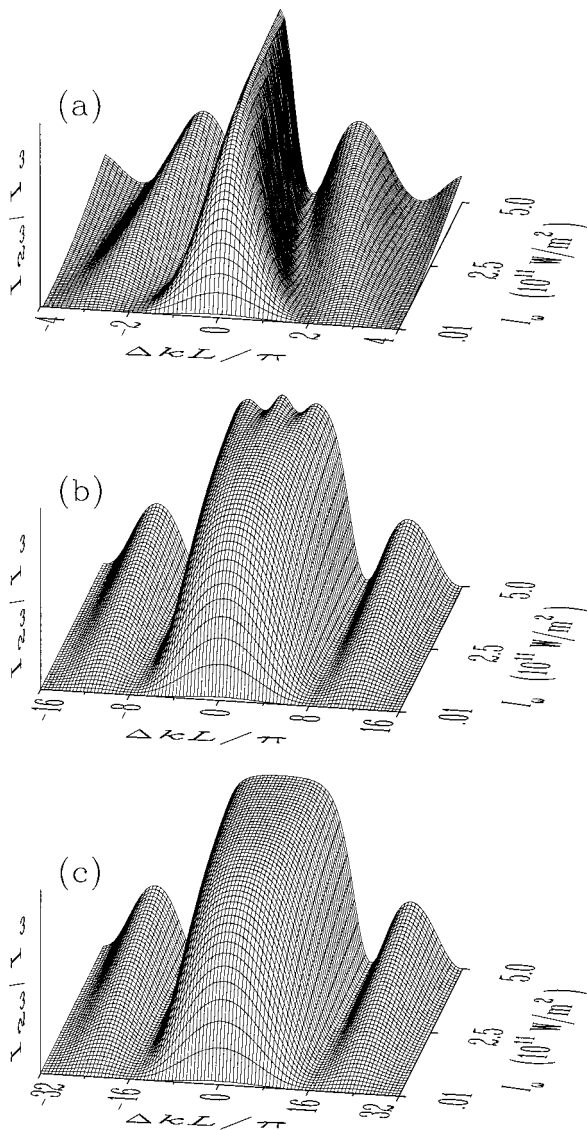


Fig. 15. Type I second-harmonic conversion efficiency of 1064-nm plane waves in 28 mm of BBO as a function of $\Delta kL/\pi$ and fundamental irradiance calculated by numeric integration (a) for a single crystal of length 28 mm, (b) for four walk-off-compensating segments of length 7 mm, and (c) for eight walk-off-compensating segments of length 3.5 mm. Note the change in the $\Delta kL/\pi$ scale.

even harder for beams with the spatial or temporal speckle discussed above in Subsection 3.D.

In Figs. 15(b) and 15(c), we explore the effect of spatial walk-off compensation for plane waves in four and eight crystal segments. Walk-off compensation is accounted for by reversing the sign of Δk in alternate segments. The crystal parameters are otherwise the same as in the top plot, but the Δk scale is expanded by four and eight. It is clear that in addition to broadening the low-irradiance acceptance angle by four or eight, walk-off compensation suppresses the narrowing at high irradiance characteristic of single crystals. Structure develops at high nonlinear drive for four segments, but it is delayed until the conversion efficiency is quite high.

We verified this behavior by using the experimental setup of Fig. 3 to compare the performance of a single

crystal with that of four walk-off-compensating segments. Figure 16(a) shows the single-crystal (actually four segments without walk-off compensation) normalized second-harmonic pulse energy (solid curves) and the depleted fundamental pulse energy (dashed curves) as a function of fundamental beam tilt. The fundamental pulse energy is 4 mJ in the lower trace, 24 mJ in the middle trace, and 44 mJ in the upper trace. The 3.3-mm beam diameter is enough larger than the 0.39-mm walk-off in a single segment that the plane-wave approximation is relevant for the walk-off-compensated case. We set the apertures of the detectors to sample only the center of the spatial Gaussian profiles. The predicted narrowing of the tilt, or Δk , tolerance with fundamental irradiance is apparent, as is the growth of the side lobes. Because the pulses are Gaussian in time rather than cw as in the calculated surfaces of Fig. 15, these traces correspond to a weighted sum of slices through the surface of Fig. 15 corresponding to different irradiances. The minima in the top plot of Fig. 15 shift with irradiance, so in the weighted sum in Fig. 16(a) they should not go to zero. This effect is apparent in the 44-mJ trace. In Fig. 16(b), the crystal is divided into four walk-off-compensating segments. The solid curves are again the

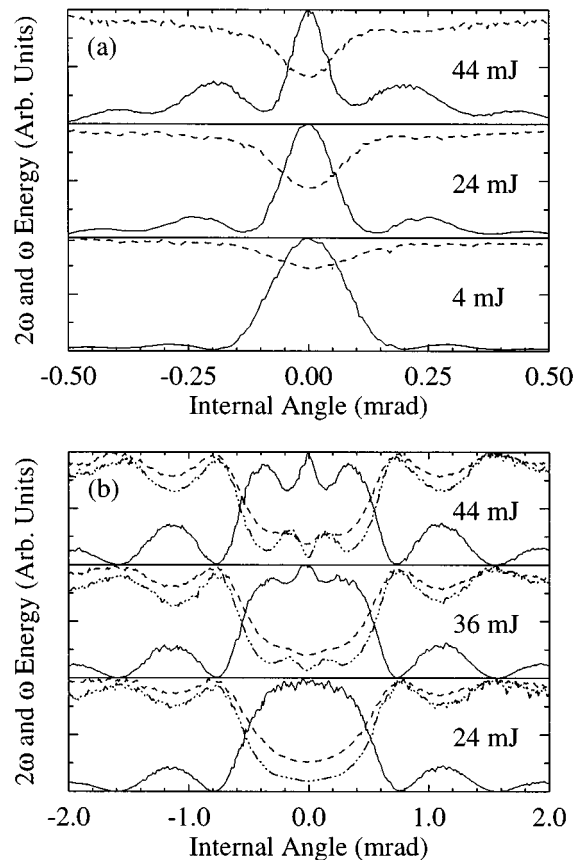


Fig. 16. Type I second-harmonic conversion efficiency of 1064-nm plane waves in 28 mm of BBO as a function of internal angle and fundamental pulse energy (a) for a single crystal of length 28 mm and (b) for four walk-off-compensating segments of length 7 mm. Solid curves are the second-harmonic fluence at the beam center, dotted-dashed curves are the depleted fundamental fluence at the beam center, and dashed curves are the depleted fundamental fluence integrated over the spatial profile.

normalized harmonic signals at beam center, the dashed-dotted curve is the depleted fundamental at beam center, and the dashed curve is the depleted fundamental integrated over the spatial profile. Clearly, segmenting the crystal provides the predicted improvement in acceptance angle relative to a single crystal. Not only is the allowable tilt angle four times as great, but it retains its width at irradiances that cause significant narrowing for the single crystal. Further, we verified the development of the three-lobed structure near $\Delta k = 0$ seen in Fig. 15(b) for four-segment compensation. Using four crystal segments, we achieved over 90% conversion at the beam center and over 80% for the whole beam. The maximum conversion without walk-off compensation was reduced because the beam diameter was increased to 4 mm to better approximate a plane wave and also because walk-off was still significant compared with the beam diameter.

Each crystal segment was aligned to $\Delta k = 0$ by maximizing second-harmonic conversion at low power where conversion was weak. We did not experimentally measure the sensitivity to misalignment of the various crystal segments, but we have modeled it with results shown in Fig. 17. Plots 17(a)–17(d) are for detuning segments 1 through 4 at the highest fundamental irradiance of Fig. 15. They indicate that alignment of the early crystal segments is more critical than alignment of the later segments, in contrast to low conversion for which the alignment of the middle segments was most critical. The alignment sensitivity of the early segments is a few times that at low conversion.

B. Collimated Gaussian Beams

We showed above that, for low-conversion type A sum-frequency mixing of collimated Gaussian beams, temporal or spatial walk-off led to a narrowing of the frequency or angular spectrum of the product light. We also showed in Figs. 15 and 16 that the permissible phase mismatch for plane waves is reduced at high nonlinear drive for a single crystal. It is reasonable to ask whether the latter effect leads to further narrowing of the product wave's frequency or angular spectrum. It is rather obvious in the local picture that narrowing of the angular spectrum cannot occur because it would imply spatial broadening of the product wave beyond the low-conversion profile, but there is no mechanism to cause such broadening. Our numerical simulations verify this. The only apparent change in the spectrum at high nonlinear drive is that slight wings are added to the low-drive spectrum of Fig. 6(a). We point this out to emphasize the difficulty of applying plane-wave analysis to real beams in strongly driven mixing. Real beams comprise an array of plane waves that are coupled by nonlinear mixing, with the result that their phases and amplitudes change as they progress through the crystal. In other words, the Fourier composition changes as the waves propagate. Reduction of the phase-mismatch tolerance can still be taken into account, but it should be considered in (x, t) space rather than in $(k, \Delta\omega)$ space. It is the local value of $\phi_{2\omega} - 2\phi_\omega$ that becomes more critical at high drive. The mixing process becomes more sensitive to any shift of this phase away from the optimal value of $\pi/2$, including shifts that are due to spatial walk-off. If $\Delta k = 0$ for the

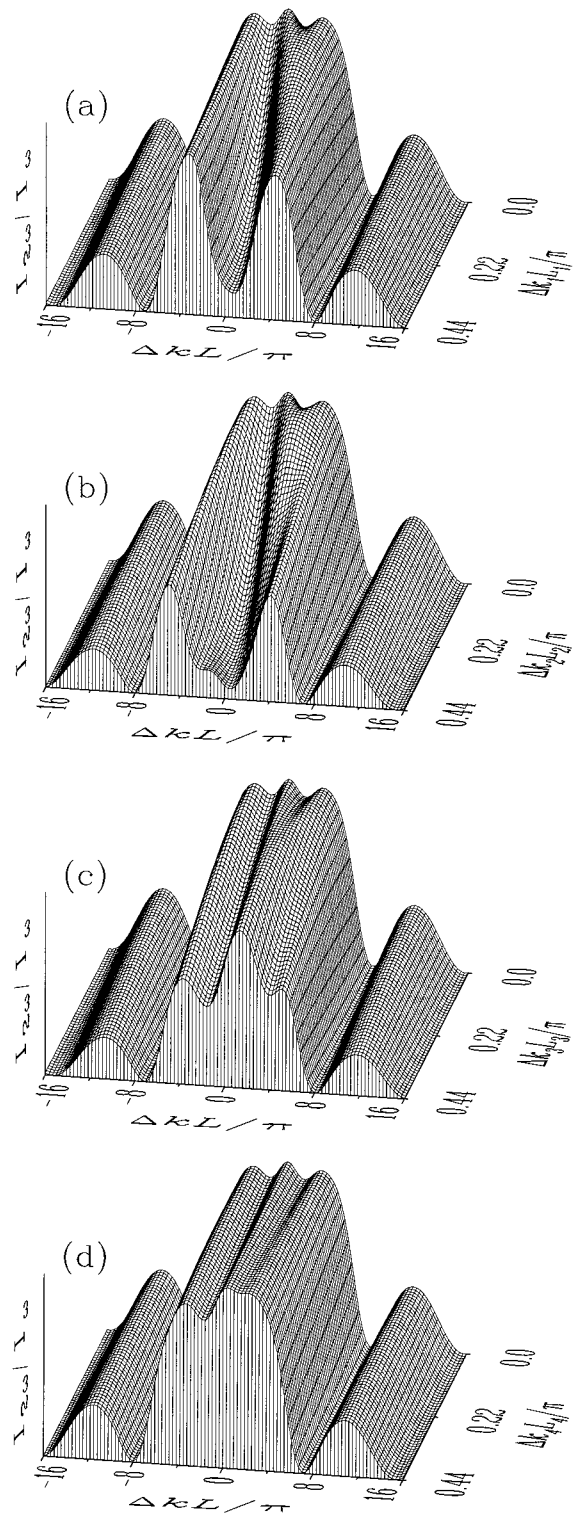


Fig. 17. Sensitivity of doubling to Δk_n , the phase mismatch of the n th crystal ($n = 1, \dots, 4$), for four walk-off-compensating crystal segments at high nonlinear drive. All crystals are adjusted to $\Delta k = 0$ except the one indicated.

carrier waves, walk-off does not cause a phase shift for collimated Gaussian beams because the phase fronts of the beams are flat, and the phase of the generated wave is independent of input irradiances. However, walk-off does cause phase shifts if $\Delta k \neq 0$ because the phase of

the generated wave is irradiance dependent. We conclude that the angular spectrum of the product wave is about the same at high or low mixing efficiency, but the sensitivity to phase-velocity mismatch of the carrier waves is greater at high nonlinear drive. This means the allowable tilt of the input beam away from the phase-match angle is reduced at high drive. Spatial walk-off compensation decreases this sensitivity, increasing the allowable carrier tilt. It also increases spatial overlap between the fundamental and harmonic beams, increasing the doubling efficiency for a given fundamental irradiance and total crystal length. Similar arguments apply to the effect of temporal walk-off on the frequency spectrum of the product wave.

C. Focused Beams

We begin by considering noncritical phase matching for which spatial walk-off is zero. There is a phase shift between the harmonic and fundamental beams because of phase shifts associated with passage through a focus. We might expect this to limit the achievable conversion efficiency because of the increased sensitivity to such phase shifts in strongly driven mixing. In fact, White *et al.*³¹ showed that this is not a serious limitation. They demonstrated by numerical modeling that a doubling efficiency of 95% is possible for cw Gaussian beams. We verified this with our model and present the results in Fig. 18. Gaussian spatial and temporal pulses can achieve 86% conversion. We also find that, at peak efficiency, the beam quality of the second harmonic is good, although the residual fundamental is quite distorted. However, if the process is overdriven, the focal phase shifts take a toll on efficiency as energy is transferred from the harmonic back to the fundamental. It may be possible to minimize the influence of the focal shifts, thus postponing backconversion, by use of segmented crystals with their individual Δk adjusted to minimize the relative phase shift between fundamental and harmonic, but we have not explored this.

There is a second source of phase shifts with focused beams introduced by spatial walk-off. The lateral shift of the curved harmonic wave front relative to the curved fundamental wave front contributes a phase shift that promotes backconversion. For example, we find by modeling that frequency doubling of 800-nm light in a 10-mm-long BBO crystal has a maximum conversion of only 61% for cw beams and 54% for Gaussian pulses. Walk-off compensation using four 2.5-mm-long segments improves these numbers to 88% for cw and 81% for pulses. The cw results are displayed in Fig. 18. Our calculation used the focal parameters of Boyd and Kleinman²¹ that would optimize low-power mixing efficiency while assuming $\rho = 70$ mrad for a single crystal and $\rho = 70/4 = 17$ mrad for four walk-off-compensating segments. We did not attempt to optimize the focusing or the values of Δk in individual crystal segments, but we believe our results are close to optimum. We conclude that walk-off compensation reduces the conversion penalty associated with walk-off of focused beams and permits efficiencies approaching those possible in noncritical frequency doubling.

D. Structured Beams

In type A frequency doubling of beams with spatial phase structure, walk-off of the harmonic beam relative to the fundamental shifts the local value of the mixing phase $\phi_{2\omega} - 2\phi_{\omega}$. The harmonic light that overlaps the fundamental at each point across the wave front was generated earlier in the crystal by fundamental light a short distance away in the negative walk-off direction. At low drive, this shift can be a significant fraction of π before it affects doubling efficiency. At high drive, the tolerance is reduced by an amount reflected in the narrowing of the phase-matching peak in Fig. 15. Consequently, small phase variations on a scale comparable to the walk-off distance ρL can substantially reduce the conversion efficiency through backconversion. That is, a small amount of light with its wave vector tilted near or outside the acceptance angle of the crystal can seriously hamper efficient mixing. This effect has been noted by Eimerl *et al.*¹⁸ in simulations of third-harmonic generation.

Similar considerations apply to temporal walk-off where temporal phase modulations on a frequency scale comparable to or greater than the crystal acceptance bandwidth can kill mixing efficiency, as noted by Eckardt and Reintjes³⁰ and by Ditmire *et al.*³² Figure 19 shows results of our simulations of frequency doubling for 2-ps Gaussian pulses, assuming a plane-wave spatial profile and assuming that group-velocity dispersion is too small to alter the pulse shapes. We compare the doubling efficiency of unmodulated pulses with that for phase- or amplitude-modulated pulses to illustrate the profound influence of slight phase distortions at high nonlinear drive. Temporal walk-off is varied while the modulation frequency is kept constant. The resulting efficiency is plotted as a function of the temporal walk-off in units of the pulse duration, $\sigma L/\tau$. Arrows at 1 and 0.55 indicate values of temporal walk-off equal to the fundamental-pulse duration and the modulation period, respectively. The solid curve for weakly driven doubling is shown for refer-

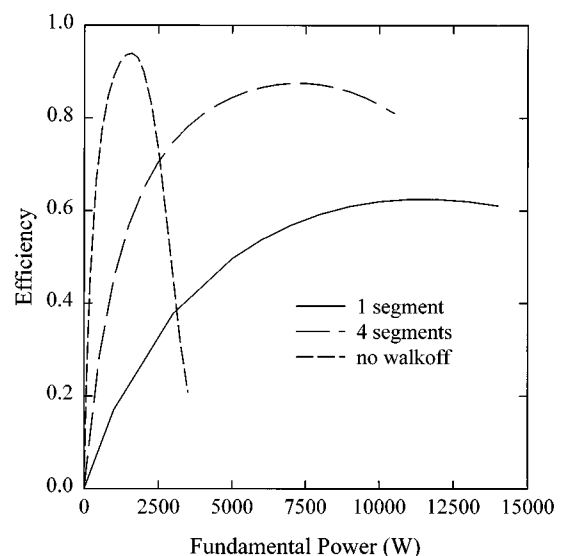


Fig. 18. Doubling efficiency of focused 800-nm beams in a 10-mm-long BBO crystal versus fundamental power for no spatial walk-off, 70-mrad walk-off in a single crystal, and 70-mrad walk-off in four walk-off-compensating crystal segments.

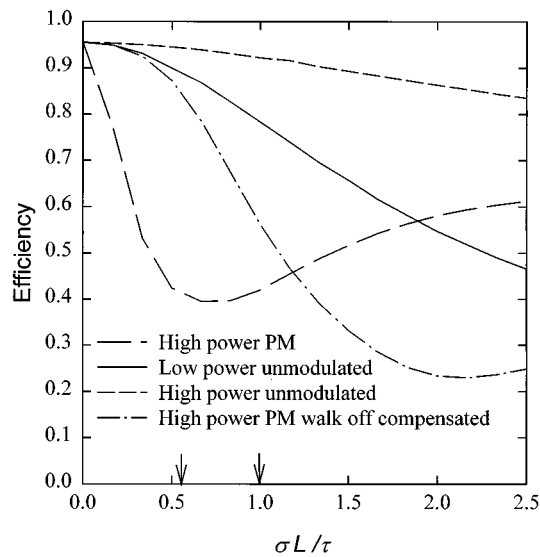


Fig. 19. Doubling efficiency versus temporal walk-off, measured in units of pulse duration, at low power normalized to 95% at $\sigma L/\tau = 0$, at high power for unmodulated pulse, for phase modulation with phase excursion of $\pi/15$ and period equal to 55% of the pulse duration in a single crystal, and for four walk-off-compensating crystal segments.

ence, normalized to the same level as the high-efficiency curves at $\sigma L/\tau = 0$. The other curves are all calculated for the fundamental pulse fluence that gives 95% conversion at $\sigma L/\tau = 0$. There are several features of interest illustrated by the figure. First, for unmodulated pulses, high-efficiency mixing (short-dashed curve) falls more slowly with increasing walk-off than does low-efficiency mixing (solid curve) because conversion takes place near the input end of the crystal before walk-off can take a toll. In contrast, if the pulse is phase modulated, the mixing efficiency falls more rapidly for strongly driven mixing than for weak mixing. The long-dashed curve represents strongly driven doubling of a pulse phase modulated with a phase excursion of $\pi/15$, which places $\sim 1\%$ of the pulse energy in each of the two sidebands, which are spaced 0.92 THz from the carrier. As the graph shows, this small phase modulation devastates doubling efficiency even for walk-off substantially less than for the modulation period, indicating that even phase shifts considerably less than $\pi/15$ substantially reduce efficiency. Temporal walk-off compensation should counter this sensitivity to phase modulation by limiting the temporal displacement between fundamental and harmonic waves. This is verified by the dotted-dashed curve for temporal walk-off compensation in four crystal segments. The allowable walk-off is about four times that for a single crystal segment. It is interesting to note that when the efficiency is reduced by phase modulation, the energy is transferred to the sidebands of the fundamental wave, as noted also by Eimerl *et al.*¹⁸ for spatial walk-off. The sidebands that started with 1% of the energy can become substantially larger than the carrier. Finally, if the fundamental wave is amplitude modulated rather than phase modulated, again with 1% of the fundamental energy in each sideband, the performance is identical to the unmodulated case (long dashed curve).

We conclude that high-conversion efficiency in type I frequency doubling demands that the phase front of the fundamental wave be very flat on the scale of the spatial walk-off and nearly chirp free on the scale of temporal walk-off. Walk-off compensation in N segments increases the tolerance to phase distortions by approximately N . Amplitude variations, in contrast, are not very important.

More generally, the sensitivity to phase variations but not amplitude variations holds for type A sum-frequency mixing as long as the input waves are photon balanced. For type B mixing, on the other hand, amplitude modulation combined with walk-off between the two input beams creates an imbalance in photon number that allows back-conversion. Thus both amplitude and phase modulation must be small for type B sum-frequency mixing, and precise photon balance must be maintained to achieve high-conversion efficiency.

6. CONCLUSIONS

We have advocated analyzing nonlinear mixing in the local (x, t) description rather than using the more common analysis in the Fourier (k, ω) description, arguing that it is less prone to misinterpretation. We have presented such an analysis in several cases of broad interest and have compared the results with the (k, ω) analysis, demonstrating their equivalence.

We have shown by analyzing four cases of low-efficiency parametric mixing that the effect of spatial (temporal) walk-off compensation in N -crystal segments can be reasonably well accounted for by replacing the walk-off $\rho(\sigma)$ with a walk-off reduced by N in expressions for acceptance angle (bandwidth) and mixing efficiency. Enhanced acceptance angles and conversion efficiency for spatial walk-off compensation was verified in a number of experiments. By analogy with the increase in acceptance angle associated with a reversal in the sign of Δk in alternating segments with spatial walk-off compensation, alternating temperature coefficients for Δk in alternate segments should increase the temperature bandwidth by N .

Similarly, the use of walk-off compensation has been shown to enhance parametric gain in the limit of low pump depletion, particularly for the pump walk-off geometry, which is useful for image amplification. We also have shown that in strongly driven sum-frequency mixing, walk-off compensation mitigates the increased sensitivity to local phase shifts between the input and product waves, allowing higher conversion for focused beams as well as for beams with less-than-ideal phase or amplitude structure.

ACKNOWLEDGMENTS

This work was supported by the U.S. Department of Energy under contract DE-AC04-94AL85000. Sandia is a multiprogram laboratory operated by Sandia Corporation, a Lockheed Martin Company, for the U.S. Department of Energy.

*Present address: WaveFront Sciences, 15100 Central Avenue SE, Albuquerque, New Mexico 87123.

REFERENCES

1. K. Hayata and M. Koshiba, "Group-velocity-matched second-harmonic generation: an efficient scheme for femtosecond ultraviolet pulse generation in periodically domain-inverted β -BaB₂O₄," *Appl. Phys. Lett.* **62**, 2188–2190 (1993).
2. C. Radzewicz, Y. B. Band, G. W. Pearson, and J. S. Krasinski, "Short pulse nonlinear frequency conversion without group-velocity-mismatch broadening," *Opt. Commun.* **117**, 295–302 (1995).
3. J. J. Zondy, M. Abed, and S. Khodja, "Twin-crystal walk-off-compensated type-II second harmonic generation: single-pass and cavity-enhanced experiments in KTiOPO₄," *J. Opt. Soc. Am. B* **11**, 2368–2379 (1994).
4. V. D. Volosov, A. G. Kalintsev, and V. N. Krylov, "Suppression of degenerate parametric processes limiting frequency-doubling efficiency of crystals," *Sov. J. Quantum Electron.* **6**, 1163–1167 (1976); V. D. Volosov, A. G. Kalintsev, and V. N. Krylov, "Degenerate parametric processes in three-wave interactions in tandem crystals," *Sov. Tech. Phys. Lett.* **2**, 32–34 (1976); V. D. Volosov and A. G. Kalintsev, "Optimum optical second-harmonic generation in tandem crystals," *Sov. Tech. Phys. Lett.* **2**, 373–375 (1976); V. D. Volosov, A. G. Kalintsev, and V. N. Krylov, "Phase effects in a double-pass frequency doubler," *Sov. Tech. Phys. Lett.* **5**, 5–7 (1979).
5. M. A. Norton, D. Eimerl, C. A. Ebberts, S. P. Velsko, and C. S. Petty, "KD*P frequency doubler for high average power applications," in *Solid State Lasers*, Proc. SPIE **1223**, 75–83 (1990).
6. R. B. Andreev, K. V. Vetrov, V. D. Volosov, and A. G. Kalintsev, "Three-wave parametric processes in multicrystal nonlinear frequency converters," *Opt. Spectrosc.* **65**, 90–93 (1988).
7. B. Ya. Zel'dovich, Yu. E. Kapitskii, and A. N. Chudinov, "Interference between second harmonics generated into different KTP crystals," *Sov. J. Quantum Electron.* **20**, 1120–1121 (1990).
8. L. K. Samanta, T. Tanagawa, and Y. Yamamoto, "Technique for enhanced second harmonic output power," *Opt. Commun.* **76**, 250–252 (1990).
9. M. Watanabe, K. Hayasaka, H. Imajo, and S. Urabe, "Continuous-wave sum-frequency generation near 194 nm with collinear double enhancement cavity," *Opt. Commun.* **97**, 225–227 (1993).
10. W. R. Bosenberg, W. S. Pelouch, and C. L. Tang, "High-efficiency and narrow-linewidth operation of a two-crystal β -BaB-2O-4 optical parametric oscillator," *Appl. Phys. Lett.* **55**, 1952–1954 (1989).
11. D. J. Armstrong, W. J. Alford, T. D. Raymond, A. V. Smith, and M. S. Bowers, "Parametric amplification and oscillation with walkoff-compensating crystals," *J. Opt. Soc. Am. B* **14**, 460–464 (1997).
12. G. T. Moore and K. Koch, "Phasing of tandem crystals for nonlinear optical frequency conversion," *Opt. Commun.* **124**, 292–294 (1996).
13. C. Xijie, D. Meilan, L. Jiapun, L. Tielxe, and Q. Wenhua, "Large-aperture high-efficiency frequency doubling using tandem KDP crystals," *Chin. Phys.* **7**, 1055–1060 (1987).
14. J.-J. Zondy, M. Abed, S. Khodja, C. Bonnin, B. Rainaud, H. Albrecht, and D. Lupinsky, "Walkoff-compensated type-I and type-II SHG using twin-crystal AgGaSe₂ and KTiOPO₄ devices," in *Nonlinear Frequency Generation and Conversion*, Proc. SPIE **2700**, 66–72 (1996).
15. J. A. Fleck, Jr. and M. D. Feit, "Beam propagation in uniaxial anisotropic media," *J. Opt. Soc. Am.* **73**, 920–926 (1983).
16. M. A. Dreger and J. K. McIver, "Second-harmonic generation in a nonlinear, anisotropic medium with diffraction and depletion," *J. Opt. Soc. Am. B* **7**, 776–784 (1990).
17. M. Trippenbach and Y. B. Band, "Propagation of light pulses in nonisotropic media," *J. Opt. Soc. Am. B* **13**, 1403–1411 (1995).
18. D. Eimerl, J. M. Auerbach, and P. W. Milonni, "Paraxial wave theory of second and third harmonic generation in uniaxial crystals," *J. Mod. Opt.* **42**, 1037–1064 (1995).
19. A. V. Smith and M. S. Bowers, "Phase distortions in sum- and difference-frequency mixing in crystals," *J. Opt. Soc. Am. B* **12**, 49–57 (1995).
20. A. V. Smith, computer code SNLO, Sandia National Laboratories, Albuquerque, N. M., 1997 (available from the authors at no charge).
21. G. D. Boyd and D. A. Kleinman, "Parametric interaction of focused Gaussian light beams," *J. Appl. Phys.* **39**, 3597–3639 (1968).
22. R. W. Boyd, *Nonlinear Optics* (Academic, New York, 1992).
23. J.-J. Zondy, "Comparative theory of walkoff-limited type-II versus type-I second harmonic generation with gaussian beams," *Opt. Commun.* **81**, 427–440 (1991).
24. J.-J. Zondy, "Experimental investigation of single and twin AgGaSe₂ crystals for CW 10.2 μ m SHG," *Opt. Commun.* **119**, 320–326 (1995).
25. J. W. Goodman, "Statistical properties of laser speckle patterns," in *Laser Speckle and Related Phenomena*, Vol. 9 of Topics in Applied Physics, J. C. Dainty, ed. (Springer-Verlag, New York, 1984).
26. B. Boulanger, J. P. Feve, G. Marnier, B. Menaert, X. Cabriol, P. Villeval, and C. Bonnin, "Relative sign and absolute magnitude of $d^{(2)}$ nonlinear coefficients of KTP from second-harmonic-generation measurements," *J. Opt. Soc. Am. B* **11**, 750–757 (1994).
27. Y. R. Shen, *The Principles of Nonlinear Optics* (Wiley, New York, 1984).
28. S. X. Dou, D. Josse, and J. Zyss, "Comparison of collinear and one-beam noncritical noncollinear phase matching in optical parametric amplification," *J. Opt. Soc. Am. B* **9**, 1312–1319 (1992).
29. E. Sidick, A. Knoesen, and A. Dienes, "Ultrashort-pulse second-harmonic generation. I. Transform-limited fundamental pulses," *J. Opt. Soc. Am. B* **12**, 1704–1712 (1995).
30. R. C. Eckardt and J. Reintjes, "Phase matching limitations of high efficiency second harmonic generation," *IEEE J. Quantum Electron.* **QE-20**, 1178–1187 (1984).
31. D. R. White, E. L. Dawes, and J. H. Marburger, "Theory of second-harmonic generation with high-conversion efficiency," *IEEE J. Quantum Electron.* **QE-6**, 793–796 (1970).
32. T. Ditmire, A. M. Rubenchik, D. Eimerl, and M. D. Perry, "Effects of cubic nonlinearity on frequency doubling of high-power laser pulses," *J. Opt. Soc. Am. B* **13**, 649–655 (1996).